Alma Mater Studiorum - Università di Bologna

SCUOLA DI SCIENZE

Dipartimento di Chimica Industriale"Toso Montanari"

Corso di Laurea Magistrale in

Chimica Industriale

Classe LM-71 - Scienze e Tecnologie della Chimica Industriale

Organic/inorganic polyoxometalate-based hybrids for oxidation catalysis and energy conversion

Tesi di laurea sperimentale

CANDIDATO

Edoardo Matricardi

RELATORE

Prof. Stefano Zacchini

CO-RELATORI

Dr. Guillaume Izzet

Dr. Geoffroy Guillemot

Sessione II

Anno Accademico 2013-2014

A mamma e babbo
e al loro sudore della fronte

TABLE OF CONTENTS

ABBREVIATIONS

POM: Polyoxometalate

TM: Transition Metal

TMSP: Transition Metal Substituted POM

FG: Functional Group

TBA: Tetrabutylammonium

DDA: Didodecyldimethylammonium

CV: Cyclic Voltammetry

DMF: Dimethylformamide

TEA: Triethylamine

[TBA]Br: Tetrabutylammonium bromide

[DDA]Br: Didodecyldimethylammonium bromide

[TBA]OH: Tetrabutylammonium hydroxide

TFA: Trifluoroacetic acid

DCM: Dichloromethane

BMIM: 1-butyl-3-methylimidazolium

ACN: Acetonitrile

DMSO: Dimethylsulphoxide

ROH: 3-methylbut-2-en-1-ol

TBHP: tert-butylhydroperoxide

MMCT transition: Metal to Metal Charge Transfer transition

ABSTRACT

This thesis work has been carried out during the Erasmus exchange period at the *"Université Paris 6 – Pierre et Marie Curie"*, in the *"Edifices PolyMétalliques – EPOM"* team, leaded by Prof. Anna Proust, belonging to the *"Institut Parisien de Chimie Moléculaire"*, under the supervision of Dr. Guillaume Izzet and Dr. Geoffroy Guillemot.

The redox properties of functionalized Keggin and Dawson POMs have been exploited in photochemical, catalytic and reactivity tests.

For the photochemical purposes, the selected POMs have been functionalized with different photoactive FGs, and the resulting products have been characterized by CV analyses, luminescence tests and UV-Vis analyses. In future, these materials will be tested for hydrogen photoproduction and polymerization of photoactive films..

For the catalytic purposes, POMs have been firstly functionalized with silanol moieties, to obtain original coordination sites, and then post-functionalized with TMs such as V, Ti and Zr in their highest oxidation states. In this way, the catalytic properties of TMs were coupled to the redox properties of POM frameworks. The redox behavior of some of these hybrids has been studied by spectro-electrochemical and EPR methods. Catalytic epoxidation tests have been carried out on allylic alcohols and n-olefins, employing different catalysts and variable amounts of them. The performances of POM-V hybrids have been compared to those of $VO(iPrO)_3$.

Finally, reactivity of POM-V^{III} hybrids has been studied, using styrene oxide and ethyl-2-diazoacetate as substrates.

All the obtained products have been analyzed *via* NMR techniques. Cyclovoltammetric analyses have been carried out in order to determine the redox behavior of selected hybrids.

1. INTRODUCTION

1.1 POLYOXOMETALATES: WHAT THEY ARE

1.1.1 Polyoxometalates as polyoxoanions

Polyoxometalates (POMs) are polyatomic ions, that consist of three or more transition metal oxoanions, linked together by sharing oxygen atoms. They are also known as "inorganic metal oxygen cluster anions". Metal atoms concerned, also called "Addenda Atoms", are these of Groups 5 and 6 of the Periodic Table, especially V, Mo and W in their highest oxidation states. Polyoxoanions are known also for metals such as Nb or Ta. The reasons why they form easily polyoxoanions are a favorable combination of ionic radius and charge, and the accessibility of empty d-orbitals for the M-O linkage.[1] These structures are considered as molecular oxide, and can incorporate several other elements of the p block or even the d block of the Periodic Table, *e.g.,* P, Si, B, Al, Ge or Co. We can divide POMs into two main categories: isopolyoxometalates, which contain only high valent transition metals of group 5 or 6 (V, Nb, Mo, W), and heteropolyoxometalates, that contain at least one other element of the block p or d. General formulas are:

- $[M_xO_y]^{n-}$ for the isopolyanions
- $[X_zM_xO_y]^{m-}$ for the heteropolyanions[2]

Transition metal (TM) atoms occupy MO_6 octahedra, which can link together by sharing verteces, edges or faces. In the octahedral cavity, not all of the oxygen atoms are shared with another TM, indeed one or two atoms are unshared and form terminal oxygen atoms. Their presence is fundamental to avoid complete condensation, as in bulk metal oxides, due to their lower basicity. Depending on the case, we can find mono-oxo species, cis-di-oxo and so on (Figure 1).

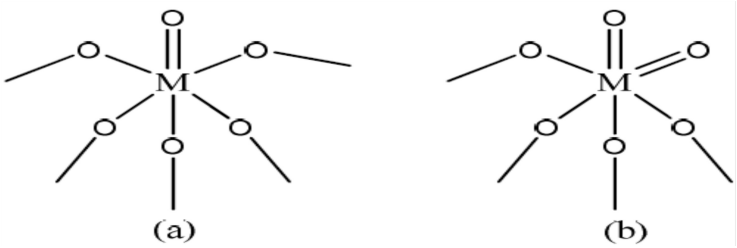

Fig. 1: a) mono-oxo species; b) cis-di-oxo species

The heteroatom of heteropolyanions can be found in a 4, 6, 8, 12 coordination environment, depending on its coordination requirements.

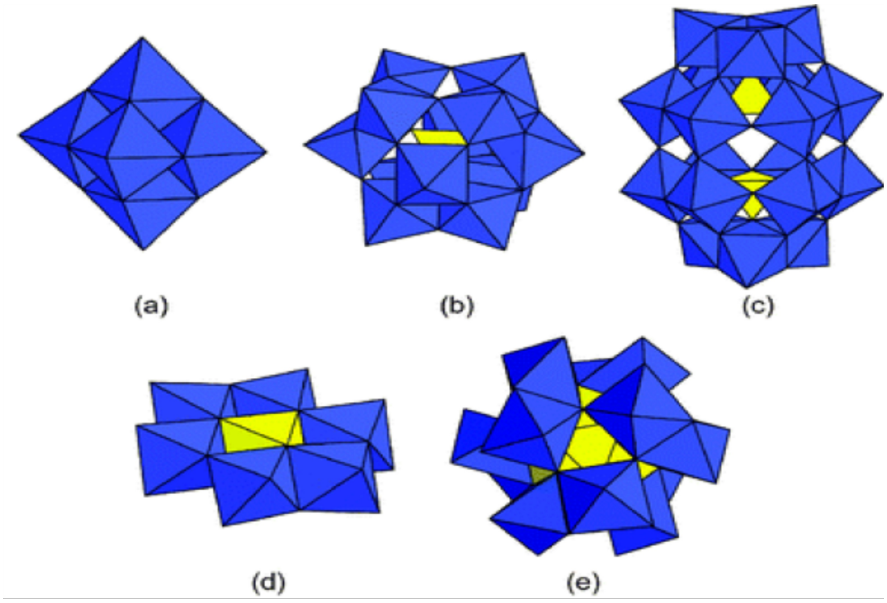

Fig. 2: POMs structures in literature: a) Lindqvist $[M_6O_{19}]^{2-}$ (M = Mo, W); b) α-Keggin $[XM_{12}O_{40}]^{n-}$ (X = P, Si, B, Al, Ge; M = Mo, W); c) α-Well-Dawson $[X_2M_{18}O_{82}]^{n-}$ (X = P, Si; M = Mo, W); d) Anderson-Evans $[XMo_6O_{24}]$ (X = P, As); e) Dexter $[XM_{12}O_{42}]^{n-i}$

In these structures, the heteroatom is contained in a central cavity, with the oxygen atoms shared with the surrounding MO_6 octahedra. The type of heteroatom depends on the size of the internal cavity, and will influence the final charge of the polyanion.[3] Among the different structures, the "α-Keggin" is one of the most studied. It is composed of four triads ($\{Mo_3O_{13}\}$ moieties) of octahedra, around a central tetrahedron, that contains the heteroatom. The octahedra in the triads are joined by edges, and the triads between them trough verteces. If we formally rotate one triad of 60°, we

can obtain up to four types of isomers. They are the isomer β, from the rotation of only one triad, γ from the rotation of two triads, δ from the rotation of three and ε from the rotation of four of them.[4]

1.1.2 Synthesis of Polyoxoanions of Cr, Mo and W

With a careful control of the experimental conditions (pH, concentration, solvent), polyoxoanions can be obtained starting from compounds of TMs.

Acidifying solutions of cromate ion, CrO_4^{2-}, yellow and tetrahedral, bicromate ion ($Cr_2O_7^{2-}$), red-orange, can be obtained. At extremely acid pH, polymeric species such as $Cr_3O_{10}^{2-}$ and $Cr_4O_{13}^{2-}$ can be obtained. These anions are formed by condensation of CrO_4 tetrahedra through verteces. The atomic dimensions of Cr do not allow formation of CrO_6 octahedra and thus no larger structures can be obtained.

Acidic solutions of Mo^{VI} and W^{VI} lead, on the contrary, to more complicated systems of polyoxoanions.

For Mo, equilibrium between the species can be reached in a few minutes, and several isopolyanions can be obtained in an acidic environment. As example:

$7[MoO_4]^{2-} + 8H^+ \rightarrow [Mo_7O_{24}]^{6-} + 4H_2O$ **(Eq. 1)**
$8[MoO_4]^{2-} + 12H^+ \rightarrow [Mo_8O_{26}]^{4-} + 4H_2O$ **(Eq. 2)**
$36[MoO_4]^{2-} + 64H^+ \rightarrow [Mo_{36}O_{112}]^{8-} + 32H_2O$ **(Eq. 3)**

The basic units of these structures are MoO_6 octahedra and MoO_4 tetrahedra. Notable quantities of strong acid are required for the condensation, because the oxygen atoms that exceed are eliminated as water molecules.

In the case of tungstate polyanions, a longer time is required in order to reach the equilibrium of condensation. From acid solutions of WO_4^{2-}, the first species obtained are paratungstates A, $[HW_6O_{21}]^{5-}$. In more acidic media, pseudo-metatungstates $[HW_6O_{20}^{3-}]_n$ are obtained. After days or weeks, aqueous solutions of these polyanions can give more complex structures, such as $[H_2W_{12}O_{42}]^{10-}$ (paratungstate B) from $[HW_6O_{21}]^{5-}$, or $[H_2W_{12}O_{40}]^{6-}$ (metatungstate, Figure 3) from $[HW_6O_{20}^{3-}]$. The metatungstate structure is the basis for the formation of Keggin type POMs.

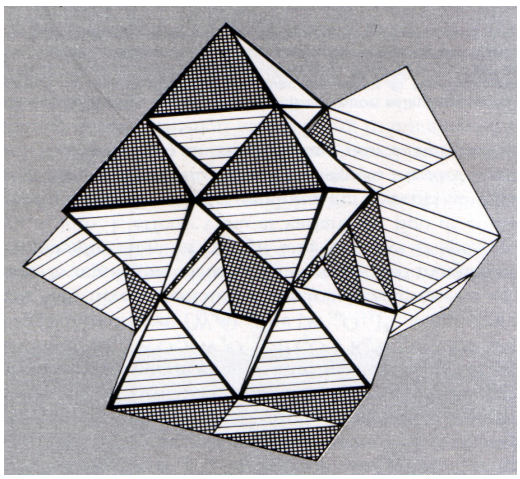

Fig. 3: Metatungstate, $[H_2W_{12}O_{40}]^{6-}$[ii]

Stop of condensation is due to electrostatic repulsion originated from metal ions at the center of condensing octahedra.

Heteropolyanions can also be obtained, derived from the condensation of polyanions with heteroatoms such as P, As, Si and Ti. The heteroatom is located in the internal cavities created by the oxygen atoms. These compounds are known mostly for Mo and W. We can find a Keggin type $[XM_{12}O_{40}]^{3-}$, suitable for small atoms such as P^V or As^V, where the heteroatom is contained in the tetrahedral central cavity formed by oxygen atoms and the final structure is analogue to that of metatungstate. As an example:

$$12MoO_4^{2-} + H_3PO_4 + 21H^+ \rightarrow [PMo_{12}O_{40}]^{3-} + 12H_2O \quad \textbf{(Eq. 4)}$$

From these structures we can originate Dawson type POMs. They are obtained from condensation of two Keggin type POM, with the loss of two triades of MO_6. The formula is $[X_2M_{18}O_{62}]^{6-}$.[5]

Structural properties, chemical behavior and compounds stability are different among metals, and it is extremely difficult to give a general description for the synthesis of POMs.[6]

1.1.3 Redox properties

The first systematic electrochemical studies on Keggin and Dawson POMs of Mo and W have been done in the 1960's. It was established with polarographic and voltammetric experiments, that POMs undergo a series of reversible and quasi-reversible reductions. Moreover, it was concluded that their redox properties strongly depended on pH. For example, reduction under acidic conditions occurs at less negative potentials, and two electrons are exchanged. Conversely, after addition of bases, the reduction potentials move to more negative values and the reduction steps become monoelectronic.[7]

POMs are chunks of metal oxides, that contain fully oxidized d^0 metal ions. Therefore, they can stabilize metals in their highest oxidation state, such as V^V, W^{VI} or Mo^{VI}. They are extremely difficult to oxidize, but they undergo reduction, yielding different colored compounds, e.g., mixed valence heteropoly "blue" and "brown". The presence of terminal oxygen atoms produces a strong axial ligand field on the metal atoms and generates a nonbonding "d_{xy}" orbital. This orbital can be occupied by new electrons, generating colored compounds. Heteropoly "blues" come from the first reduction, and ESR studies show the paramagnetic nature of these ions. In this way we can generate several Mo^V or W^V for each polyanionic compound. The blue color arises from enhanced d-d transitions and inter-valence charge transfer bands, or rather metal to metal charge transfer bands (MMTC) between the reduced M^V and oxidized M^{VI} centers. Intra-ionic disproportion under acidic conditions of "blues" generates further reduction and consequently heteropoly "brown" species. These species contain metal-metal bonded triangular clusters of $W^{IV}O_6$ octahedra. To keep the anion charge low, each W^{IV} bears a terminal H_2O ligand, and the $W^{IV}(H_2O)$ group may be oxidized back to W^{VI} *via* atom-transfer with, for instance, Me_2SO:

$$[(SiO_4)W_9O_{33}\{W^{IV}(H_2O)\}_3]^{4-} + 3Me_2SO \rightarrow [(SiO_4)W_{12}O_{36}]^{4-} + 3Me_2S + 3H_2O \quad \textbf{(Eq.5)}^3$$

1.1.4 Applications

Special properties of POMs (protons and electron storage, size, high molecular weight and so on) lead to many application fields. The first kind of application was in analitical chemistry, for example in phosphate and silicate determination via "heteropoly blue" formation. Nowadays, the largest application field of POMs is catalysis, *e.g.* in the

oxidation of methacrolein to methacrylic acid, methane oxidation or Wacker chemistry processes. Other applications are as stain for electron microscopy, as phasing agents for structural cristallography of large molecules, for the selective inhibition of enzyme function or utilization of their potent antitumoral and antiviral activity.[8]

The application field related to our work, is the utilization of POMs in redox catalysis and for artificial photosynthesis studies, thanks to their property of electrons storage and transfer.

1.2 POLYOXOMETALATES FUNCTIONALIZATION

1.2.1 Polyoxometalates functionalization via electrostatic interactions

POMs functionalization represents an important step to allow their use and integration in functional architectures and devices. It also affords new chemical properties and widens the application fields of these compounds.

Since POMs are negatively charged molecules, the first strategy of functionalization was the exchange of the counter-ion. It allows, first, to change the solubility of the compound, depending on the polarity and the organic/inorganic nature of the cation. Examples are their immobilization on many surfaces such as positively charged polyelectrolytes, surfactant-encapsulated POMs as optical or catalytic materials or electrostatic embedding of POMs into polymers. Other ways of functionalisation via non-covalent linkages are represented by the immobilization of POMs on graphite and metal surfaces, for microscopy imaging, or immobilization of POMs on carbon nanotubes.[8]

1.2.2 Polyoxometalates functionalization via covalent interactions

Another possibility of functionalization of POMs consists in covalent linkage. It offers many advantages: better control of interactions between components, rational design of molecular assemblies, better dispersion of POMs in matrices and improvement in long-term stability of the assembly.

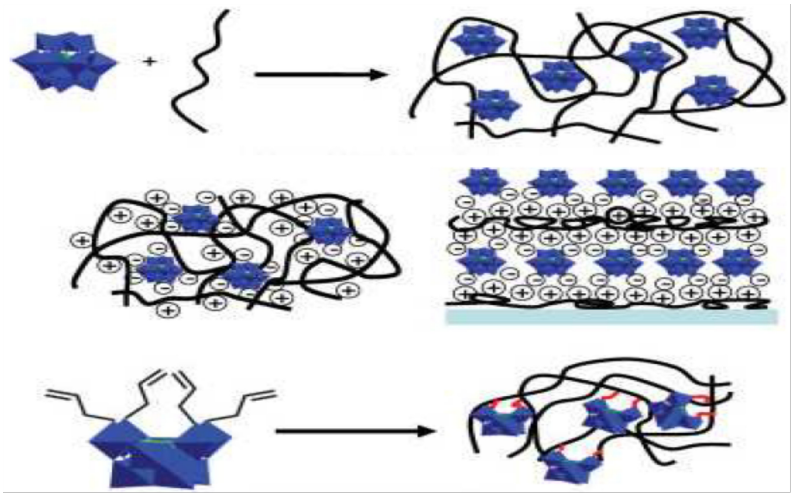

Figure 4: Different ways of functionalization of POMs: Physical trapping, Electrostatic and Covalent Bonding[iii]

In order to functionalize the starting POM, it is necessary, first, to obtain an intermediate lacunary species, which is, successively, functionalized. A lacunary POM is a chemical species deprived of one or more MO_6 octahedral units. This species can be obtained by treatment of the starting POM with a mild base such as bicarbonate.

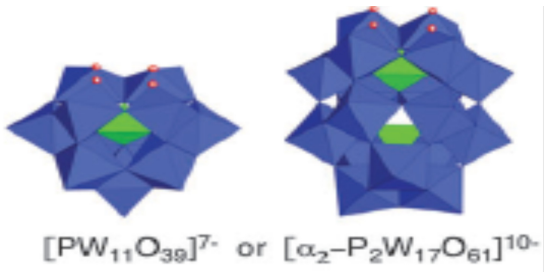

Figure 5: Example of monovacant "Keggin" and "Dawson" POMs[iv]

The so obtained lacunary POMs contain terminal oxygen atoms with enhanced nucleophilic character. These, in turn, may react with elctrophilic species such as organosilanes, organotin, transition metal complexes or organometallic compounds. After this step, a post-functionalization is possible, leading to compounds with new properties, allowing for example the immobilization of POMs on a surface or developing new utilizations in many fields, such as nanosciences or catalysis.

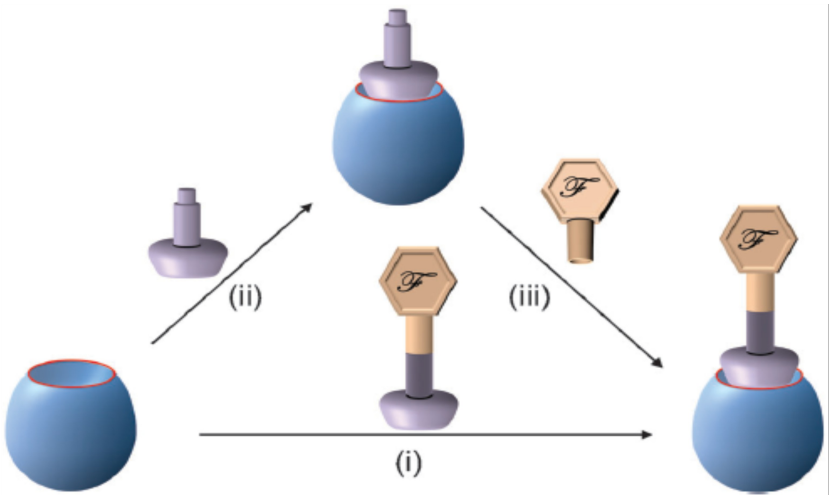

Figure 6: Different routes for the synthesis of POM organic-inorgnic hybrids. Path (i): direct functionalization, paths (ii, iii): post-functionalization. Lacunary POM is represented in blue, the anchoring tether is lilac and the added functional moiety is beige.[iv]

The lacunary POMs can be reacted with TM complexes in order to obtain functionalized species. To date, there are examples of all the first raw TM which have been included into POMs. The resulting TMSPs displays a variety of new properties, such as magnetic properties and catalytic activities. In a similar way, it is also possible to functionalize POMs with organometallic compounds.[9]

1.3 PHOTOSENSIBILIZED POMs FOR APPLICATIONS IN ARTIFICIAL PHOTOSYNTESIS

1.3.1 Natural and artificial photosynthesis

Photosynthesis is the natural process with which plants produce glucose and oxygen starting from carbon dioxide and water. The general equation of photosynthesis is:

$$6CO_2 + 6H_2O \rightarrow C_6H_{12}O_6 + 6O_2 \quad \textbf{(Eq. 6)}$$

It involves water oxidation, with oxygen production, and simultaneously the reduction of carbon dioxide, to produce glucose. The process is divided in “light reaction” and “light-independent reaction”. In the former phase, photons excite the

"photosystem II", that takes electrons coming from water oxidation and passes them through different proteins with decreasing potentials, up to "photosystem I", to produce finally ATP and NADPH. The latter molecules will be used, in the "light-independent reaction", to reduce CO_2 and produce glucose and other bio-molecules, according to the Calvin Cycle (Figure 7).[10]

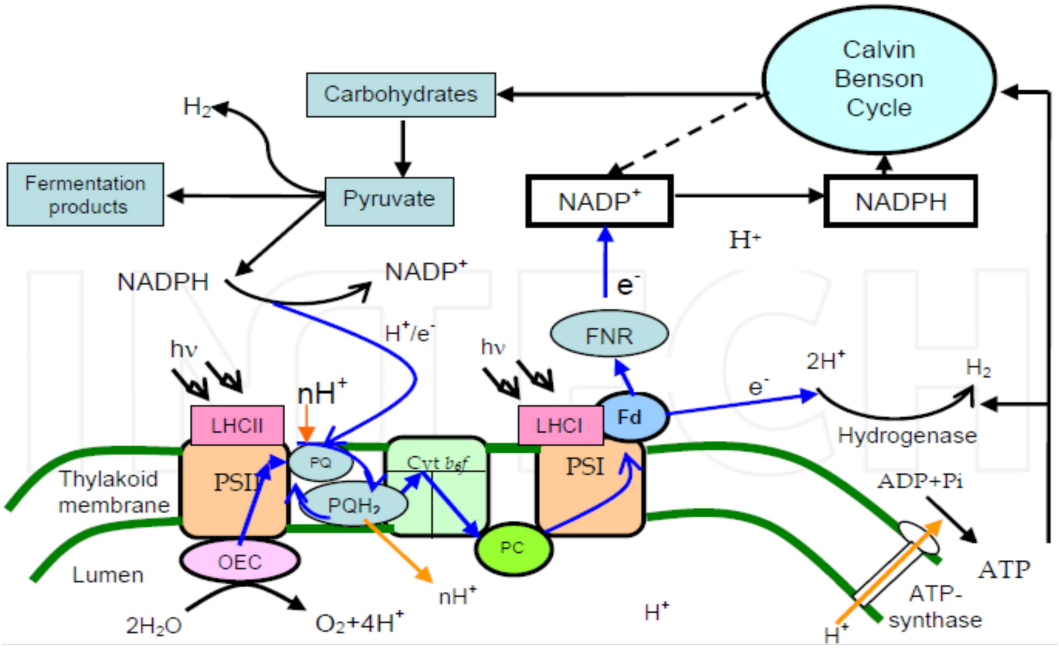

Figure7: Photosynthetical cycles[v]

The reproduction in laboratory of photosynthesis is called artificial photosynthesis. Artificial photosynthesis research projects generally try to convert solar energy into fuels, with greater efficiency than photovoltaic systems or biomass combustion.[11]

Several research lines are conducted, for example in photoelectrochemical cell or photocatalytic water splitting. Among them, the photoproduction of hydrogen is a field of extreme interest. The considered reaction is the water splitting, where the reduction of CO_2 that occurs in photosynthesis is replaced by the reduction of H^+:

$$H_2O \rightarrow H_2 + 1/2O_2 \quad \textbf{(Eq. 7)}$$

Pure water absorbs light only in the infrared region, where the energies are too low to allow water splitting. Thus a molecule able to absorb in the UV-Vis region, such as a TM complex or an organic dye, must be employed. Since a photon is able to stimulate

the release of only one electron, while the oxidation process requires two electrons for each oxygen atom, a chemical species able to store electrons is also needed. Totally, the system will be composed by an "antenna", able to convert the absorbed photons into emitted electrons, a reduction catalyst and an oxidation catalyst. Either the full redox reaction or the two half-reactions separately are studied, the latter by utilizing a sacrificial electron donor or acceptor.[12] POMs may be used as reduction catalysts, thanks to their electron storage properties and the ability of their reduced forms to produce hydrogen from protons. Hydrogen evolution has already been observed from photo-activation of "Transition Metal Substituted Polyoxometalates" (TMSPs), in the presence of protons and a sacrificial reductant, such as water. Since POMs have empty d-orbitals, the photochemical process is an LMCT transfer, lying in the UV-Vis part of spectrum.[9]

1.4 GENERATION OF COORDINATION SITES FOR POMs APPLICATIONS IN CATALYSIS

1.4.1 POMs and TMs for catalytic applications

Another field of great interest in POMs applications is catalysis, both homogeneous and heterogeneous. Molybdophosphates have been already used in the oxidation of methacrolein to methacrylic acid, and in methane oxidation. Molybdovanadophosphates are used in the Wacker process, in the oxidation of alkenes and coupling of aromatics.[8] Doping with TMs is a good strategy to improve catalytic properties. An electrostatic coordination is possible, and there are several examples. However, the best way is the covalent bonding on lacunary polyanions, to obtain TMSPs. In this way, the redox properties of POMs are coupled to the catalytic properties of TMs. Lacunary polyanions derive from the corresponding saturated POM, after the removal of one or more octahedral MO_6 unit, under basic conditions. This treatment affords terminal nucleophilic oxygen atoms and creates a polydentate site, able to coordinate one or more TMs, such as Fe, Mn, Zr or V. There are two modes of coordination: the first is called "in-pocket", and consists of substitution of one addenda atom with another TM atom; the second is called "out-of-pocket", with the new TM atom that occupies a vacancy without being completely embedded. This second way allows to obtain "sandwich" structures, where the TM bridges two vacant POMs sub-units, or other larger molecular architectures

stabilized by two or more vacant sub-units. The nucleophilicity of terminal oxygen atoms can be also exploited for reactions with electrophilic organic molecules in order to obtain organic-inorganic hybrid complexes.[13]

1.4.2 POMs functionalization with silanol moieties

POMs functionalization with sterically bulky silanol moieties can afford new and original coordination sites for catalytic applications. Sterically protected well defined single metal sites can be obtained, opening new perspectives in organometallic chemistry. Indeed, if silanol GFs, for example, with -OH functions are used, a post-functionalization is possible. As the POM is composed of d^0 metals, it can allow for example metal-ligand multiple bond formation (metal-oxo, metal-nitrene, metal-carbene).[14] As an example, reaction of the dilacunary γ-$[PW_{10}O_{36}]^{7-}$ with tert-butylsilane affords a hybrid POM that presents a rigid bis-silanol coordination environment (Figure 8). [15]

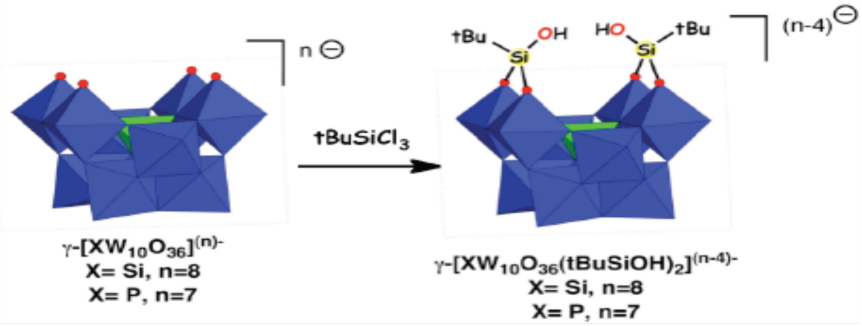

Fig. 8: Silanol functionalization

Moreover, the silanol groups of modified POMs may mimic the silanol groups present on silica surfaces, largely applied in organometallic catalysis. Then, once an organometallic compound is coupled to such silanol modified POMs, the resulting compound may be viewed as a molecular analogous of an organometallic complex bonded to a silica surface. It is noteworthy that molecular species can be separated and characterized more easily than surface complexes. As an example, studies have already been done on catalytic olefin epoxidation on alkoxi-titanium surface complexes. Mono, bis and tripodal alkoxide titanium complexes have been analyzed, and the best activity was found in tripodal titanium, where there is the best compromise between the accessibility of metal center and its increase in electrophilicity.[16] Metal oxides

substitution with POMs can represent, in this field, an interesting development, thanks to electron storage properties of these compounds.

2. OBJECTIVE

2.1 POMs FUNCTIONALIZATION FOR PHOTOCATALYTIC APPLICATIONS

Due to their electron storage properties, POMs have been studied for hydrogen photoproduction.

Keggin and Dawson type POMs covalently grafted to heteroleptic cyclometalated Ir^{III} complexes have been already prepared, by postfunctionalization of organosylil and organotin POM derivatives. Combined transient absorption and spectroelectrochemical measurements provided evidence of photoinduced electron transfer from the cromophore GF to the POM.[17]

Redox properties of covalent Ir^{III}-photosynthesized polyoxotungstates have been already tested. The system was found to be able to perform photocatalytic hydrogen production under visible light, thank to the decisive effect of the covalent bonding between the POM and the photosensitizer.[18]

However, Ir complexes already selected and developed present a weak hydrolysis resistance, and our aim is to carry out new functionalization with other kinds of complexes and to accomplish new photochemical and photocatalytic studies.

Another field developed is POM covalent post-functionalization with pyridyl groups, in order to obtain photoactive films *via* polymerization with metal porphyrins.
They have been already obtained by the electro-oxidation of zinc octaethylporphyrinin the presence of a Dawson type polyoxophosphovanadotungstate bearing two pyridyl groups, and their electrochemical properties studied.[19] In this Thesis, new kinds of POM were employed in the post-functionalization with pyridyl groups, with the aim to obtain new photocatalytic films.

2.2 SYNTHESIS OF NEW PHOTOSENSITIZED POM-BASED HYBRIDS FOR HYDROGEN PHOTOPRODUCTION

In this work, new photosensitized POM-based hybrids were obtained, trough Sonogashira coupling reaction, carried out on iodo-aril derivatives of Keggin and Dawson POMs hybrids[20]. The new compounds were obtained by post-functionalization with photoactive FGs, such as Ir^{III} complexes and pyridyl groups, and the electrochemical properties of products were analyzed. The four selected hybrids are:

- $[TBA]_4[PW_{11}O_{39}Sn(pC_6H_4I)]$ (**K_{Sn}^{W}[I]**)
- $[TBA]_4[PMo_{11}O_{39}Sn(pC_6H_4I)]$ (**K_{sn}^{Mo}[I]**)
- $[TBA]_6[P_2W_{17}O_{62}(Si(pC_6H_4I))_2]$ (**D_{Si}^{W}[I]**)
- $[TBA]_3[PW_{11}O_{40}(Si(pC_6H_4I))_2]$ (**K_{si}^{W}[I]**)

where D and K mean Dawson and Keggin type; Si, Sn and I indicate the kind of first functionalization (the atoms present in the FG); and W and Mo indicate the metal of the POM backbone. The counter-ion of starting POMs is tetrabutylammonium (TBA). The two selected FGs are 1-ethynylpyrydine (**Pyr**) and ethynyl-IrOxazole (**IrOxa**) (Figure 9):

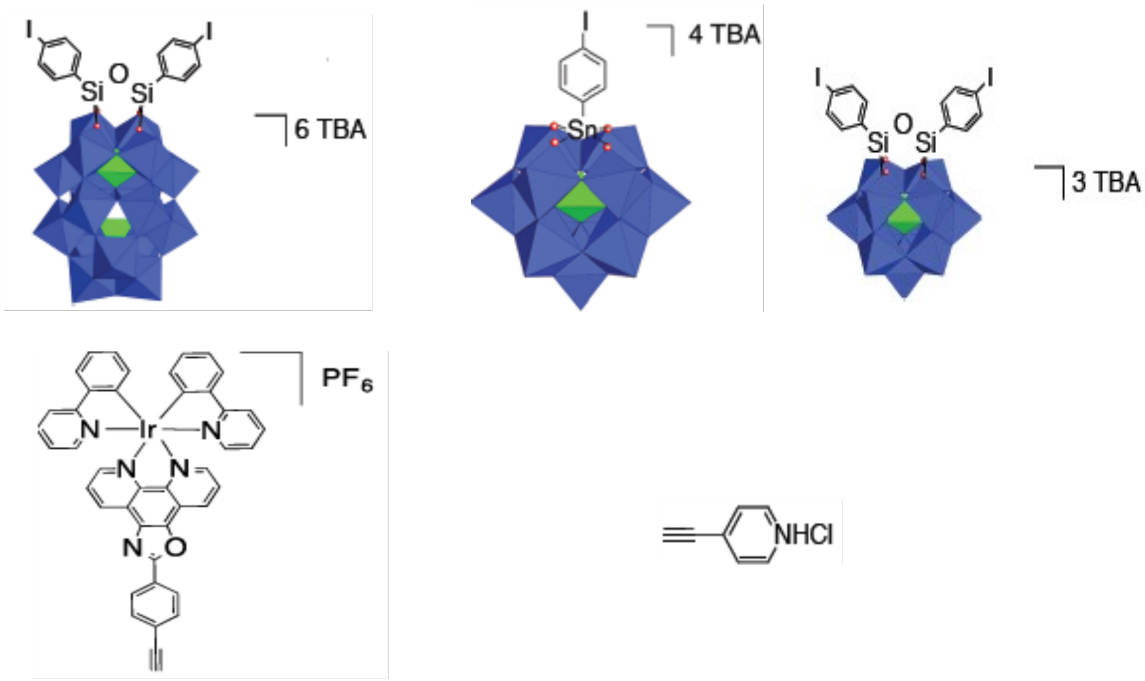

Fig. 9: In the order: $[TBA]_6[P_2W_{17}O_{62}(Si(pC_6H_4I))_2]$ or D_{si}^{W}[I], $[TBA]_4[PMo_{11}O_{39}Sn(pC_6H_4I)]$ or K_{sn}^{Mo}[I] and $[TBA]_4[PW_{11}O_{39}Sn(pC_6H_4I)]$ or K_{Sn}^{W} [I], $[TBA]_3[PW_{11}O_{40}(Si(pC_6H_4I))_2]$ or K_{si}^{W}[I], [IrOxa] complex and [Pyr] group

The Sonogashira cross-coupling reaction allowed to bond photoactive complexes on the organic-inorganic hybrids obtained. Four reactions were carried out:

- K_{Sn}^{W} [I]+ [IrOxa]
- K_{Sn}^{Mo}[I] + [IrOxa]

- D_{Si}^{W}[I] + [Pyr]
- K_{Si}^{W}[I] + [Pyr]

Post-functionalization with pyridyl moieties afforded bifunctional species, that then will be employed for the polimerization of photoactive POM films; post-functionalization with Ir complex afforded monofunctional species, that will be tested in photocatalytic hydrogen production.

Focus: Sonogashira cross-coupling reaction

The Sonogashira cross-coupling reaction is the coupling of terminal alkynes with aryl or vinyl halides, under palladium catalysis. The catalyst is a Pd (0) species, and the co-catalyst is copper (I) iodide, in the presence of a base. According to the mechanism, deprotonation of alkynes takes place, followed by substitution of proton with a Cu atom. On the Pd (0) centre, an oxydative addition of the aryl alide occurs, to obtain a Pd (II) species; the subsequent step is a terminal coordination of alkynyl copper to the metal center (transmetallation). Finally, a reductive elimination takes place on the metal centre, generating Pd (0) and coupling of the organic ligands to obtain the final organic product (Figure 10).[21]

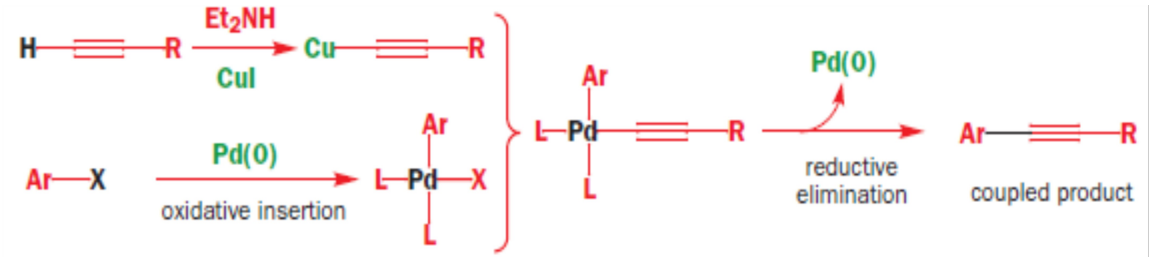

Fig. 10: General mechanism of Sonogashira coupling reaction[vi]

The Sonogashira cross-coupling reaction was first reported by Kenkichi Sonogashira, Yasuo Tohda, and Nobue Hagihara in their 1975 publication.[22] It was a remarkable discovery because it is a coupling that can be carried out at room temperature and it allows to couple organic moieties to obtain bigger and more complex molecules and products.

2.4 SYNTHESIS OF POMS FOR CATALYTIC OXIDATION PROCESSES AND REACTIVITY TESTS

In this part of the work, redox properties of POMs were studied and exploited to manage some reactivity and catalytic tests, and these properties were coupled with those of early transition metals. Studied TMs were V^{III}, V^{V}, Zr^{IV} and Ti^{IV}. As an example, vanadium oxide is already employed in catalytic oxidation processes, such as SO_2 oxidation or allylic alcohol epoxidation.[23] Vanadium phosphor oxides are also used in C_4 fraction oxidation to maleic anhydride.[24]

Coupling of catalytic properties of TM and redox properties of POM were analyzed, in an original sterically protected coordination environment due to bis- and tris-silanol first functionalization. Catalytic and reactivity tests with small molecules were carried out; for the former, metals in their highest oxidation states were used, while for the latter metals in intermediate oxidation states were employed.

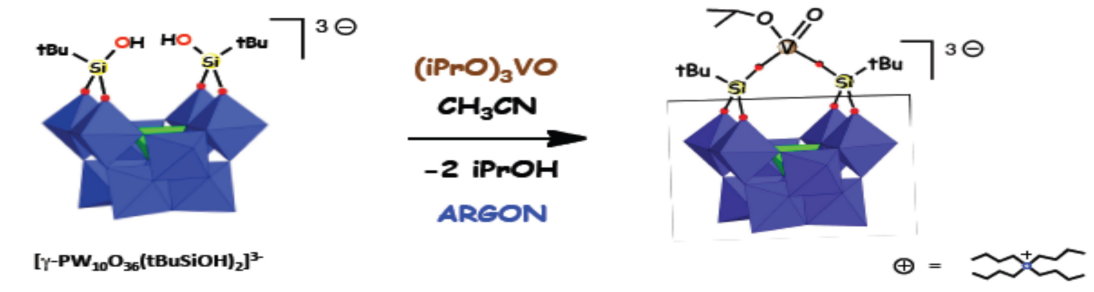

Fig. 11: Example of reaction with redox-active TM

Electrochemical tests were also performed, such as CV and UV-Vis-spectroelectrochemistry coupled analyses. ^{1}H, ^{31}P and ^{51}V NMR techniques were employed, and EPR analyses were also accomplished.

3. RESULTS AND DISCUSSION

3.1 POMs POST-FUNCTIONALIZATION FOR HYDROGEN PHOTOPRODUCTION

Among other possibilities, POMs were selected for the synthesis of photoactive molecules because of their properties of electron reservoir and redox behavior. Keggin and Dawson heteropolytungstates (derived from $[PW_{12}O_{40}]^{3-}$ and $[P_2W_{18}O_{62}]^{6-}$ POMs, respectively) and Keggin heteropolymolybdates (derived from $[PMo_{12}O_{40}]^{3-}$) were chosen, since the obtained hybrids show substantial hydrolytic and thermal resistance. Complete POMs are not suitable for this kind of functionalization, since terminal oxygen atoms are rather weak nucleophiles. However, lacunary polyanions react readily with several species such as metal complexes or electrophilic organic moieties, since they have unsatured oxygen atoms. In a previous work, lacunary polyanions (Keggin and Dawson types) were firstly functionalizated with organosilyl and organotin groups (see 2.OBJECTIVE).

A covalent-type of functionalization was chosen, instead of a non-covalent one. The latter solution is more developed and exploited, but the former one presents several advantages: among others, it allows, to enhance directionality and the interaction between the organic and inorganic components.

All the syntheses were conducted in a Schlenk tube under argon atmosphere, to avoid oxidation and contamination of starting products. The utilization of a microwave reactor allowed to reduce the reaction time up to one hour, at 80°C.

The Sonoghashira cross-coupling reaction was used in the post-functionalization step, with Pd(0) as catalyst and CuI as co-catalyst. A base was necessary to deprotonate the terminal alkyne, and freshly distilled Et_3N was used (Figure 12).

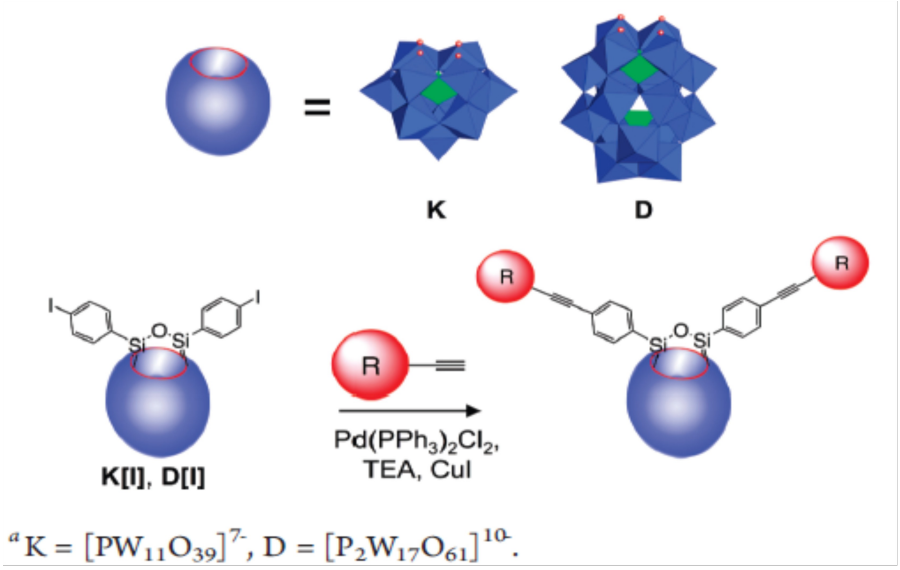

Fig. 12: Example of post-functionalization path[vii]

The purification of the reaction products was obtained by selective precipitation on the basis of their differential solubility on miscellaneous solvents. The nature of the counter-ion has a strong influence on the solubility properties of POMs: an organic counter-ion, like TBA, makes the POM soluble in organic and polar solvents, like DMSO and ACN. To allow purification, less polar solvents were progressively used to dissolve the reaction product and separate impurities. In this way it is hard to obtain very high yields, but, on the other hand, the obtained products are rather pure. The scale of solvents used, in order of decreasing solubility, is

$$DMSO > CH_3CN > EtOH > Et_2O$$

The products were characterized *via* ^{1}H and ^{31}P NMR.

Photochemical tests were carried out on post-functionalized POMs. CV analyses were performed in order to study the redox properties of the products. The redox properties were investigated in the presence or not of a source of acids, in order to determine the effect of the presence of protons on the reduction potentials and the nature of the reduction steps. After that, the products were submitted to other tests at Jena University, by the team of Prof. B. Dietzek. In particular, UV-Vis spectra were recorded and luminescence tests were accomplished. Photolysis studies in the presence of protons

and sacrificial electron donors, for hydrogen photoproduction, will be tested in the future, at CEA of Grenoble. Polymerization of POM-pyridyl hybrids will be also tested in the future, to obtain photoactive POM films.

- **Synthesis and characterization of $[BMIM]_3[PW_{11}O_{39}Sn(p\text{-}C_6H_4\text{-}ethynyl\text{-}IrOxazole)]$ (K_{Sn}^{W} [IrOxa])**

K_{sn}^{W}[IrOxa] is a post-functionalized Keggin type POM, obtained from the coupling of $[TBA]_4[PW_{11}O_{39}Sn(pC_6H_4I)]$ (**K_{Sn}^{W}[I]**) with an Ir Oxazole complex (Figure 13).

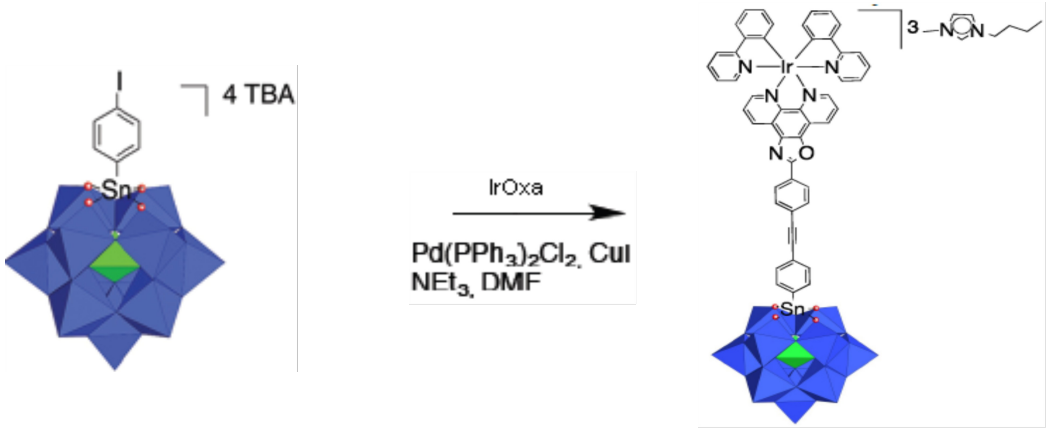

Fig. 13 Synthesis of K_{Sn}^{W} [IrOxa]. On the left, K_{sn}^{W}[I], on the right K_{Sn}^{W} [IrOxa]

After the reaction, the TBA counter-ion was exchanged with 1-butyl-3-methylimidazolium (BMIM). The reaction product was characterized *via* ^{1}H NMR spectroscopy (Figure 14).

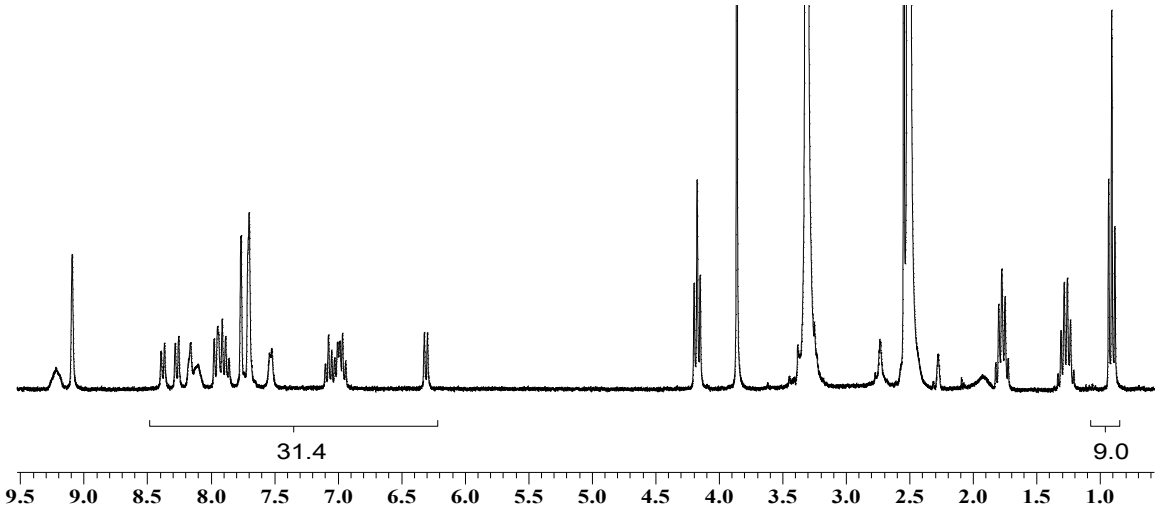

Fig. 14: ^{1}H NMR spectrum of K_{Sn}^{W} [IrOxa]

The BMIM cation displays its typical resonances at δ 1.0, 1.4, 1.8 and 4.2 ppm, whereas the aromatic protons of the FG resonate at 6-9 ppm. Integration of the aromatic protons of FG vs. the protons of BMIM results in a 31.4:9 ratio, in good agreement with the 3- charge of **K_{Sn}^{W} [IrOxa].**

The CV analysis was carried out with different concentrations of acid or base (Figure 15). The blue line was obtained with **K_{sn}^{W}[IrOxa]** 1 mM, the red one with the addition of 1 equivalent of TBAOH and the yellow one with 250 equivalents of TFA.

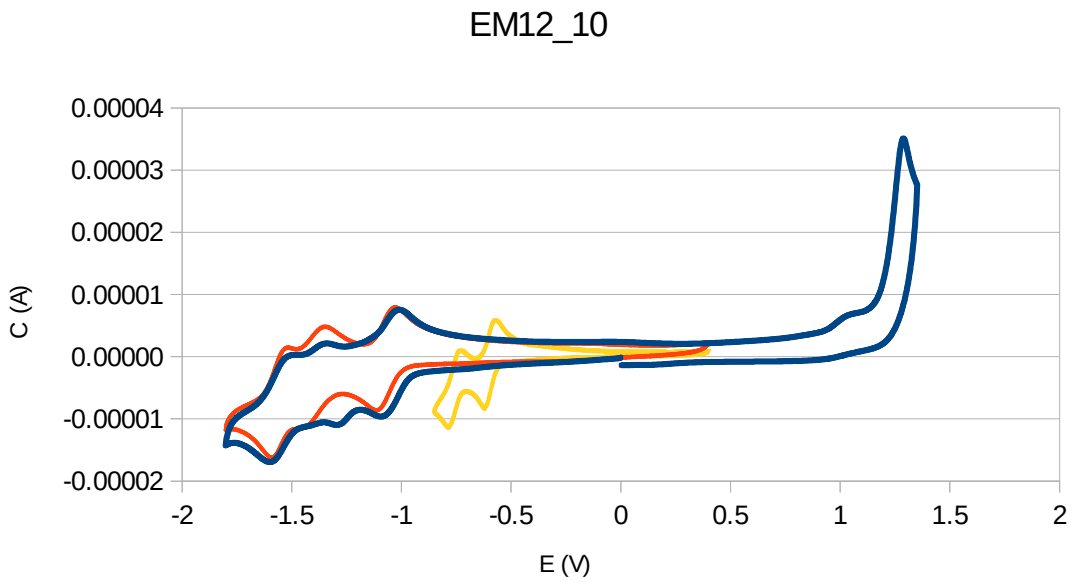

Fig. 15: CV of K_{Sn}^{W} [IrOxa]. Blue: POM 1 mM, Red: 1 eq TBAOH, Yellow: 250 eq TFA. DMF containing 0.1 M of $TBAPF_6$. Working electrode, glassy carbon; reference electrode, SCE; counter-electrode, Pt wire.

K_{sn}^{W}[Ir_{oxa}] (blue line) displays a reversible process at -1.05 V vs SCE attributable to the first monoelectronic reduction of the tungstic framework followed by several broad waves between -1.2 V and -1.5 V vs SCE corresponding to the further reduction of the POM and the protonated Iridium complex. Upon addition of 1 equiv. of TBAOH, **K_{Sn}^{W}[Ir_{oxa}]** displays three reversible waves at *ca.* -1.07 V, -1.40 V and -1.55 V vs SCE attributed to the two first mono-electronic reductions of the tungstic framework and the reduction of the deprotonated iridium complex respectively. Progressive addition of TFA (up to 250 equiv.) results in a continuous shift of the reduction potentials towards less

negative values. Moreover, in the presence of an excess of TFA the reduction processes become bi-electronic as indicated by the gradual increase of the intensity of the voltammetric waves. The presence of protons modifies the redox behavior of the POM as a consequence of a counter-cation exchange. In the case of acid environment, a better definition of redox waves and their shift at higher potentials can be noted.

The formal electrode potentials (E°' vs. SCE) (for 250 eq. of TFA) are:

1. $E°'(3^{-}/5^{-}) = -0.600$ V
2. $E°'(5^{-}/7^{-}) = -0.754$ V

UV-Vis analysis and luminescence tests were carried out at Jena University.

The UV-vis spectra of $\mathbf{K_{Sn}{}^{W}[Ir_{oxa}]}$ have been performed in DMF at a concentration of 0.1 mM. The visible absorptions features of the iridium chromophore $\mathbf{[Ir_{oxa}]}$ are located in the 400-500 nm region and are assigned to singlet–singlet and formally spin forbidden singlet–triplet metal to ligand transitions. These bands are drastically affected by the presence of protons (TFA) and bases (triethylamine) (Figures 16 and 18).

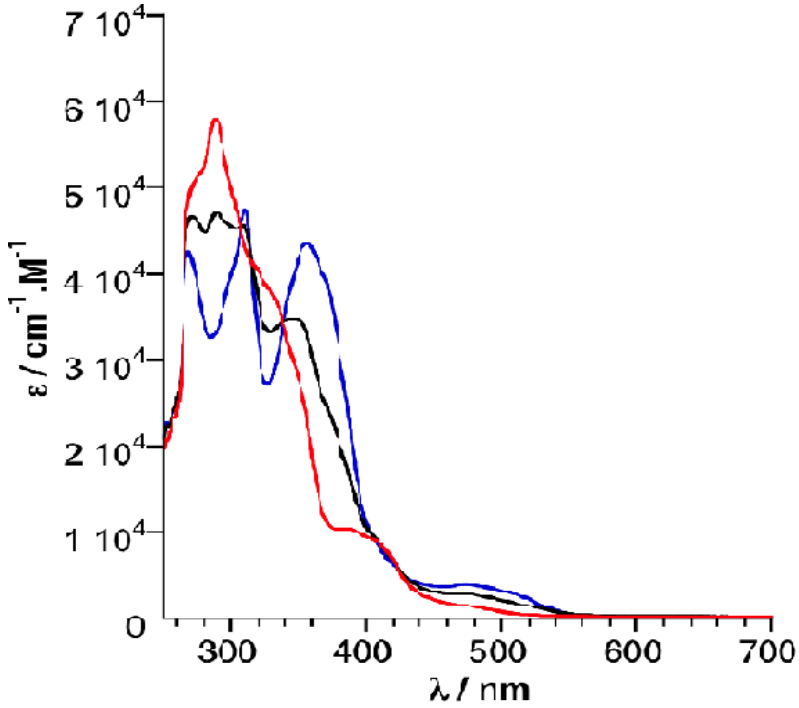

Fig. 16: Absorption spectra of [Iroxa] in DMF solutions (black), with TFA (red) and with TEA (blue)

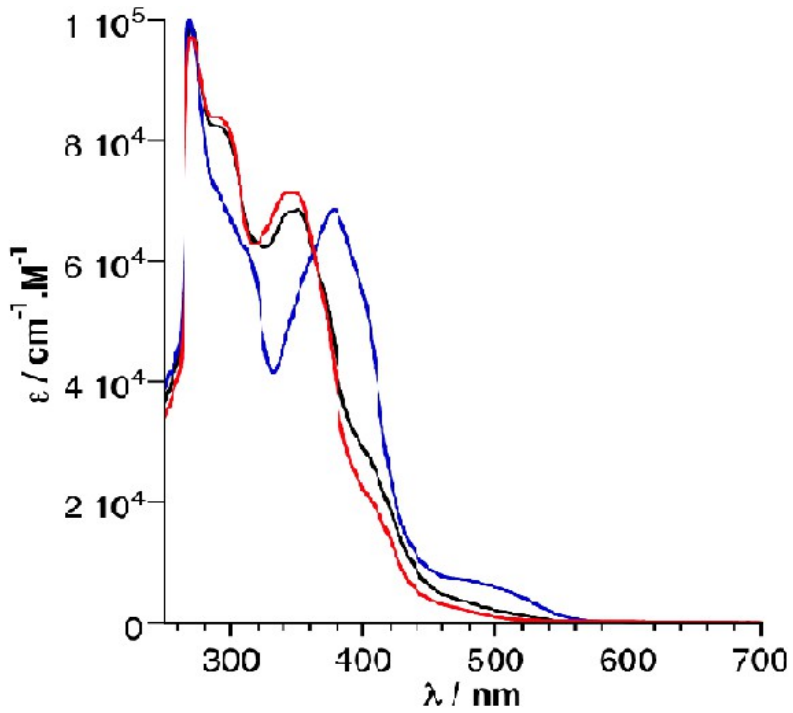

Fig. 18: Absorption spectra of K_{Sn}^{W}[Iroxa] in DMF solutions (black), with TFA (red) and with TEA (blue)

The presence of isobestic points in the iridium reference **[IrOxa]** indicates that it is partially protoned on the oxazole linker. The presence of traces of protons, coming from traces of water, in DMF is however not excluded. A special care to remove the possible traces of protons in the DMF solutions has to be taken in the future. The visible absorption spectra of reported POM–Ir dyad are dominated by the carbocyclometalated Ir(III) chromophore units, since the POM itself does not contribute to the spectral profile in the visible region. The addition of trifluoroacetic acid mostly does not affect the UV-vis spectrum of the hybrids, which indicates that they are fully protonated after their synthesis.

The iridium reference **[Ir_{oxa}]** in DMF solutions displays emission spectra centred at 589 nm following its excitation at 410 nm. Upon the addition of few equiv. of TFA, the emission of the reference complex is drastically enhanced, while the shape of the emission spectrum is barely unaffected. This suggests that the emission of the Ir complex arises from its protonated form, the unprotonated form being not luminescent.

The tungstic POM-based hybrid **K_{Sn}^{W}[Ir_{oxa}]** displays similar luminescence following its excitation at 410 nm (λ = 589 nm) with approximately the same intensity than that of the free iridium complex. This suggests that, the charge injection on the POM is negligible or slow. Considering the oxidation potential of the iridium complex, it seems likely that the photoexcited iridium complex is not sufficiently reductive to perform a photo-induced electron transfer to the POM. Upon the addition of a very large excess of TFA (>100000 equiv.), we observed a decay of 50 to 75 % of the initial luminescence that may be attributed to a partial charge injection on the POM (note that the emission of the Ir reference complex is also partially quenched upon addition of such quantity of TFA).

- **Synthesis and characterization of $[BMIM]_3[PMo_{11}O_{39}Sn(p\text{-}C_6H_4\text{-}ethynyl\text{-}IrOxazole)]$ K_{Sn}^{Mo} [IrOxa]**

K_{Sn}^{Mo}[IrOxa] is a mono-functional Keggin type POM, and was obtained from the coupling of $[TBA]_4[PMo_{11}O_{39}Sn(pC_6H_4I)]$ (**K_{Sn}^{Mo}[I]**) with an Ir Oxazole complex (Figure 19).

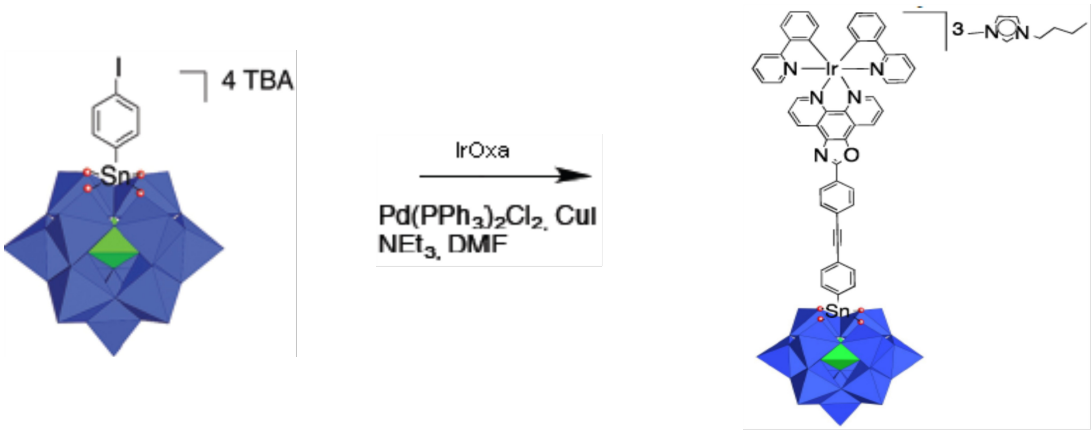

Fig. 19 Synthesis of K_{Sn}^{Mo} [IrOxa]. On the left, K_{Sn}^{Mo}[I], on the right K_{Sn}^{Mo} [IrOxa]

The reaction product was identified *via* ^{1}H and ^{31}P NMR. The ^{1}H spectrum is similar to that of **K_{Sn}^{W} [IrOxa]**. The ^{31}P spectrum displays a singlet for the inner P of the POM framework, at δ -2.9 ppm. The presence of a single resonance in the ^{31}P NMR spectrum indicates that the product has been obtained rather pure.

The CV analysis was carried out with different concentrations of acid or base. (figure 20). The blue line was obtained with $\mathbf{K_{Sn}^{Mo}}$ **[IrOxa]** 1 mM, the red one with the addition of 1 equivalent of TBAOH and the black one with 250 equivalents of TFA.

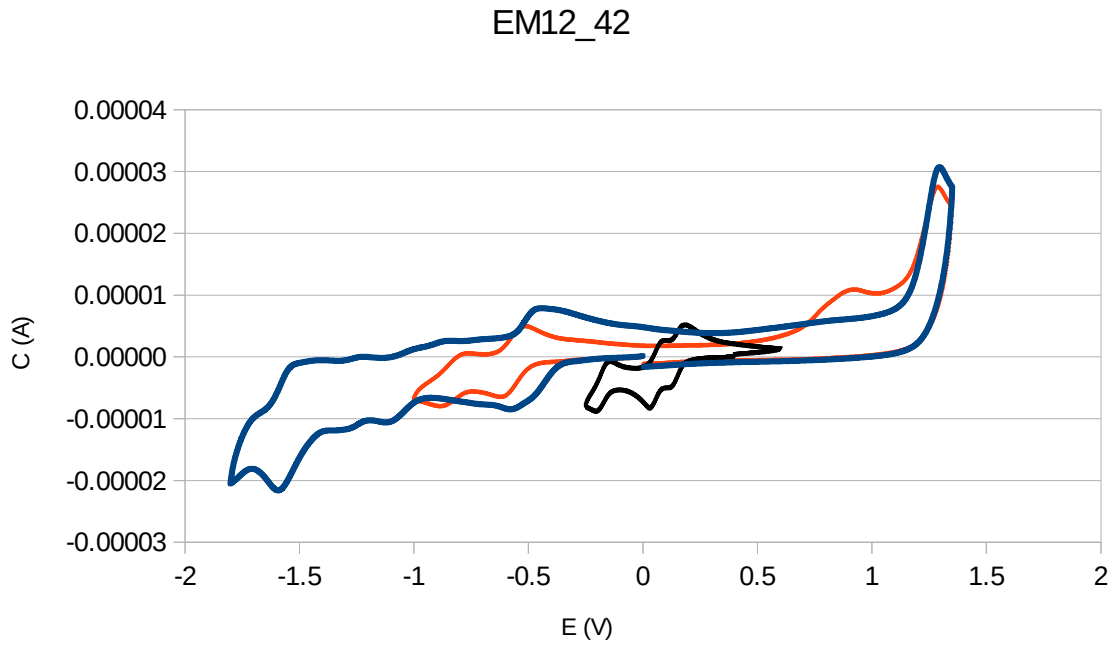

Fig. 20: CV of K_{Sn}^{Mo}[IrOxa]. Blue: POM 1 mM, Red: 1 eq TBAOH, Black: 250 eq TFA. DMF containing 0.1 M of $TBAPF_6$. Working electrode, glassy carbon; reference electrode, SCE; counter-electrode, Pt wire.

The electrochemical behavior of $\mathbf{K_{Sn}^{Mo}[Ir_{oxa}]}$ follows the same trend as that of its tungstic POM-based hybrid analog $\mathbf{K_{Sn}^{W}[Ir_{oxa}]}$. Initially the hybrid displays a first ill-defined reduction process at -0.51 V vs SCE, due to the presence of protons coming from impurities. After the addition of TFA (from 8 to 250 equiv.), three reversible reduction waves, assigned to two-electron reduction processes of the molybdic framework, continuously shift towards positive potentials.

The formal electrode potentials (E°' vs. SCE) (for 250 eq. of TFA) are:

1. E'°(-3/-5) = 0.170 V
2. E'°(-5/-7) = 0.050 V
3. E'°(-7/-9) = -0.200 V

Luminescence tests were carried out at Jena University.

The molybdic hybrid $\mathbf{K_{Sn}^{Mo}[Ir_{oxa}]}$ displays a poor emission centred at 590 nm after excitation at 410 nm (*ca.* 20 times less intense than that of $\mathbf{[Ir_{oxa}]}$). This emission is further quenched upon the progressive addition of TFA (Figure X). After the addition of 50 eq. of TFA, a residual emission is still observed and does not decay significantly upon the further addition of TFA. The quenching process in this case is likely an electron transfer from the iridium chromophore to the POM (Figure 21).

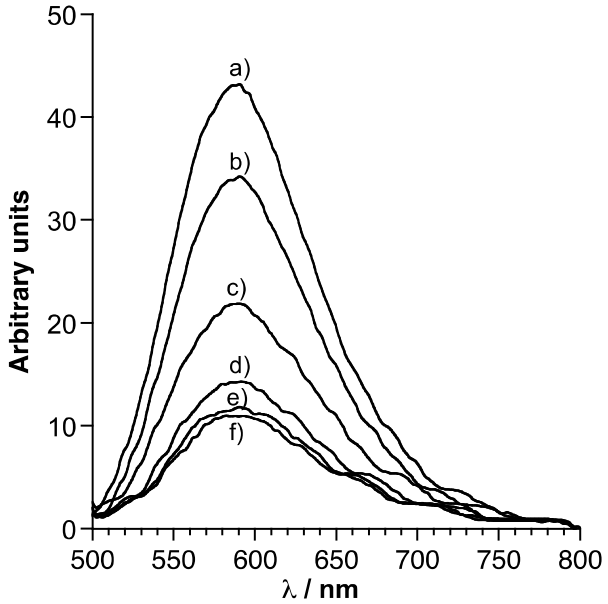

Fig. 21: Evolution of the luminescence (λ exc = 410 nm) of a solution of K_{Sn}^{Mo}[Iroxa] in DMF upon the addition of TFA: a) 3 equiv., b) 6 equiv., c) 10 equiv., d) 25 equiv.,,e) 50 equiv., f) 100 equiv..

Charge photoaccumulation and hydrogen photoproduction of $\mathbf{K_{sn}^{Mo}[IrOxa]}$ are currently under investigation.

- **Synthesis and characterization of $\mathbf{[TBA]_6[P_2W_{17}O_{62}(Si\text{-}C_6H_4\text{-}ethynylPyr)_2]}$ $\mathbf{(D_{si}^{W}[Pyr]_2)}$**

$\mathbf{D_{si}^{W}[Pyr]_2}$ is a bi-functional Dawson type POM, and was obtained from the coupling of $[TBA]_6[P_2W_{17}O_{62}(Si(pC_6H_4I))_2]$ ($\mathbf{D_{si}^{W}[I]}$) with two ethynyl-pyridine FGs (figure 22).

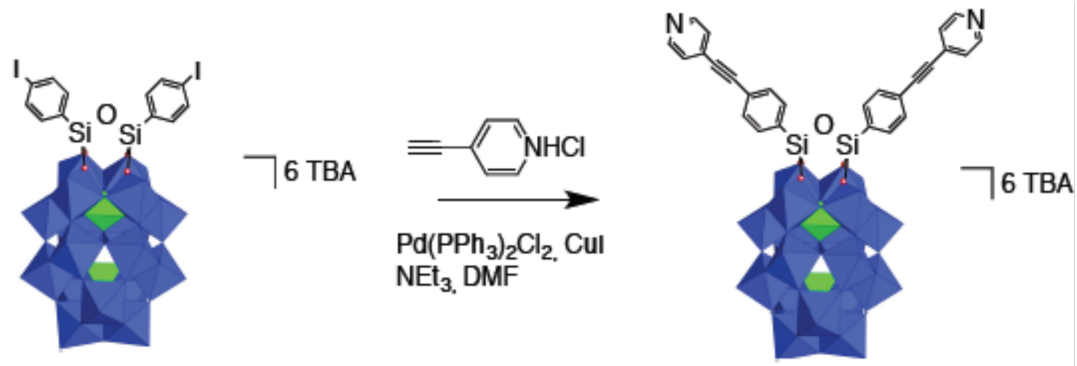

Fig. 22: Synthesis of $D_{si}^{W}[Pyr]_2$. On the left $D_{si}^{W}[I]$, on the right $D_{si}^{W}[Pyr]_2$

The reaction product was characterized *via* ^{1}H NMR (figure 23).

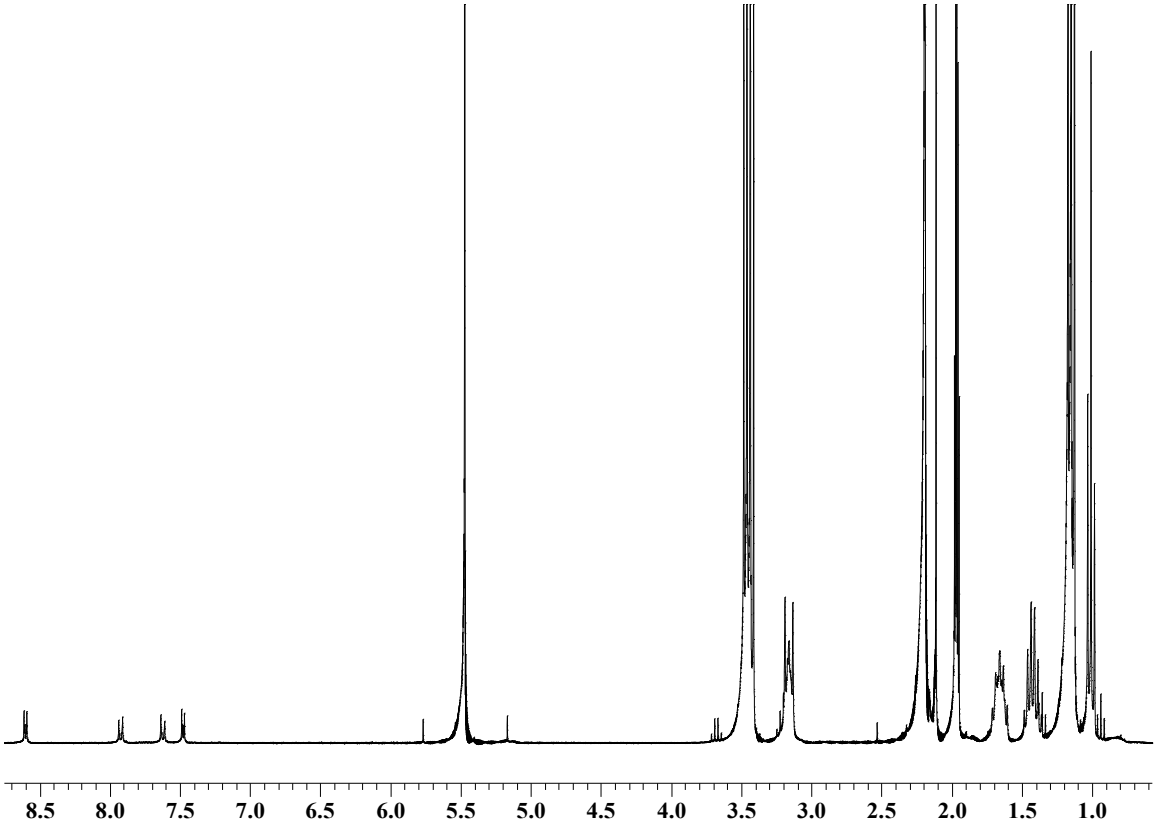

Fig. 23: ^{1}H NMR spectrum of $D_{si}^{W}[Pyr]_2$

In the ^{1}H spectrum, we can observe at δ 1.00, 1.50, 1.70 and 3.15 ppm the resonances of TBA, and between 7.5 and 8.6 ppm the aromatic resonances of the FG.

Four monoelectronic redox processes, with features of chemical reversibility, are present in the cathodic part of the cyclic voltammogramm (Figure 24).

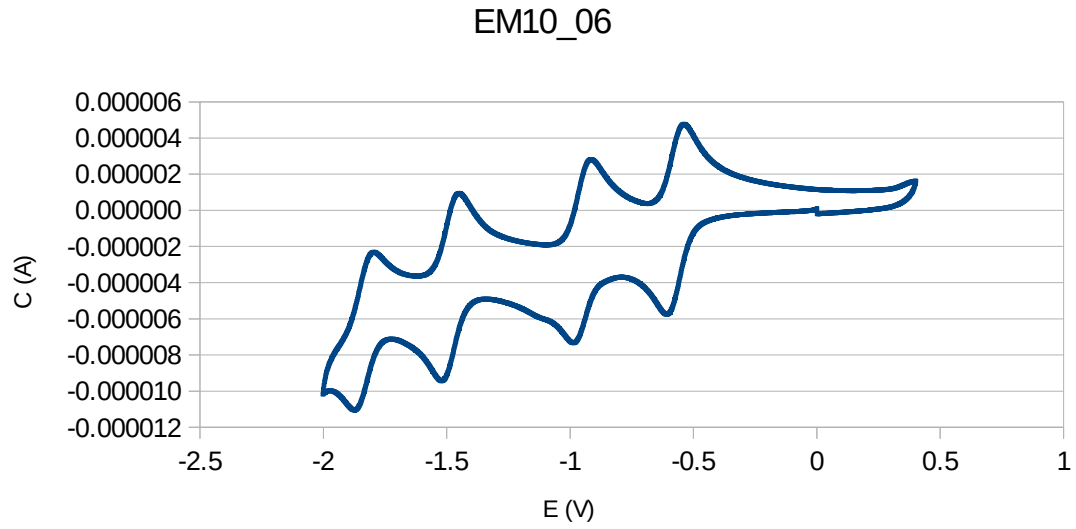

Fig. 24: CV of $D_{si}^{W}[Pyr]_2$. DMF containing 0.1 M of $TBAPF_6$. Working electrode, glassy carbon; reference electrode, SCE; counter-electrode, Pt wire.

This corresponds to the sequential monoelectronic reduction of the hexa-anion down to the deca-anion.

The formal electrode potentials (E° vs. SCE) are:

1. $E°'(6^-/7^-) = -0.586$ V
2. $E°'(7^-/8^-) = -0.965$ V
3. $E°'(8^-/9^-) = -1.498$ V
4. $E°'(9^-/10^-) = -1.857$ V

According to the literature, the reduction processes are centered on the POM.[25]

- **Synthesis and characterization of $[TBA]_3[PW_{11}O_{40}(Si\text{-}C_6H_4\text{-}ethynylPyr)_2]$ ($K_{sn}^{W}[Pyr]_2$)**

$K_{sn}^{W}[Pyr]_2$ is a bi-functional Keggin type POM, and was obtained from the coupling of $[TBA]_3[PW_{11}O_{40}(Si(pC_6H_4I))_2]$ (**$K_{sn}^{W}[I]$**) with two ethynyl-pyridine FGs (Figure 25).

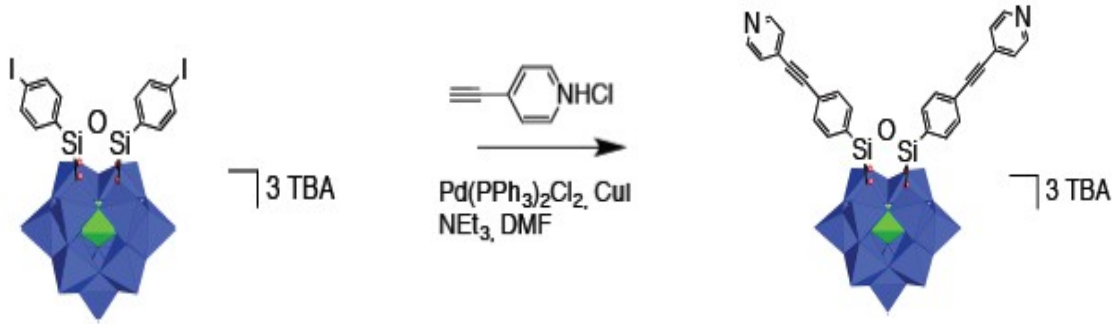

Fig. 25 Synthesis of K_{Si}^{W} [Pyr]$_2$

The reaction product was characterized *via* ^{1}H and ^{31}P NMR. The ^{1}H spectrum is similar to that of $\mathbf{D_{Si}^{W}}$ **[Pyr]$_2$**, and the ^{31}P spectrum gave one main singlet for the inner P of the POM framework, at δ -13.30 ppm.

From the CV analysis, three monoelectronic reversible redox processes can be recognized in the cathodic region (figure 26).

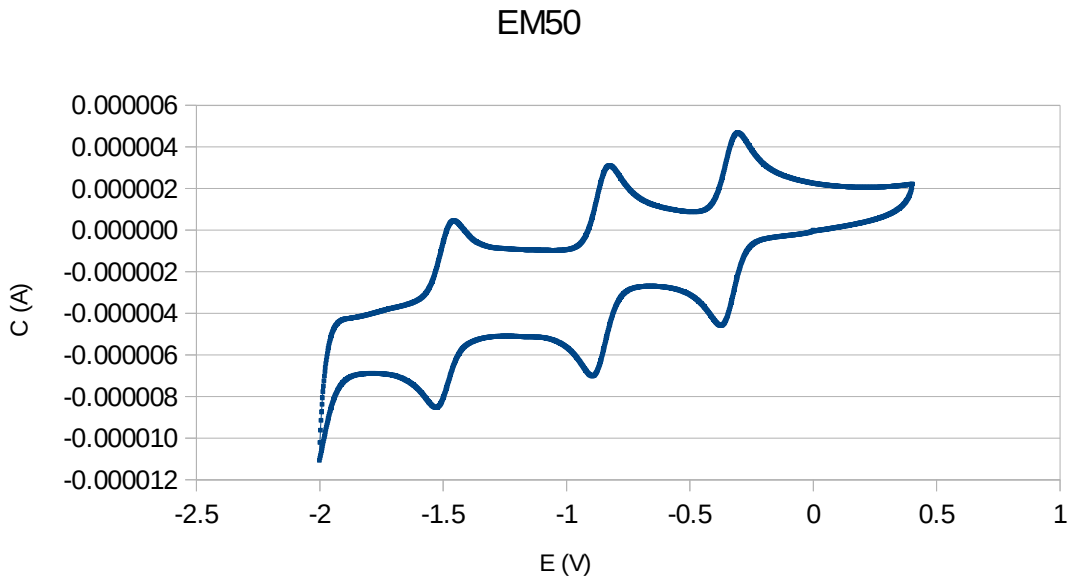

Fig. 26: CV of K_{Sn}^{W}[Pyr]$_2$. DMF containing 0.1 M of TBAPF$_6$. Working electrode, glassy carbon; reference electrode, SCE; counter-electrode, Pt wire.

The formal electrode potentials (E° vs. SCE) are:

1. $E^{\circ\prime}(4^{-}/5^{-})$ = -0.325 V

2. $E°'(5^-/6^-) = -0.880$ V
3. $E°'(6^-/7^-) = -1.510$ V

According to the literature, the reduction processes are POM centered.[26]

3.2 POMs FUNCTIONALIZATION FOR CATALYTICAL APPLICATIONS AND REACTIVITY STUDIES

Catalysis is one of the most known application field of POMs. To carry out catalytic and reactivity studies, redox active Keggin type POMs have been coupled to catalytic active early TMs.

3.2.1 Generation of organosilanol coordination sites on lacunary POMs

Two main coordination environments were used, bis-silanol and tris-silanol. These FGs were introduced by reacting POMs with ^{t}BuSiCl$_3$. In this way, rigid and stable coordination sites with new redox and structural properties were obtained, as reported in the literature.[26]

The lacunary POMs employed were $Cs_7[PW_{10}O_{36}]$ (**PW10**) and $K_9[PW_9O_{34}]$ (**PW9**), resulting after reaction with ^{t}BuSiCl$_3$ in their functionalized forms $[TBA]_3[PW_{10}O_{36}(^t BuSiOH)_2]$ (**PW10Si2**) and $[TBA]_3[PW_9O_{34}(^t BuSiOH)_3]$ (**PW9Si3**), respectively (Figure 27).

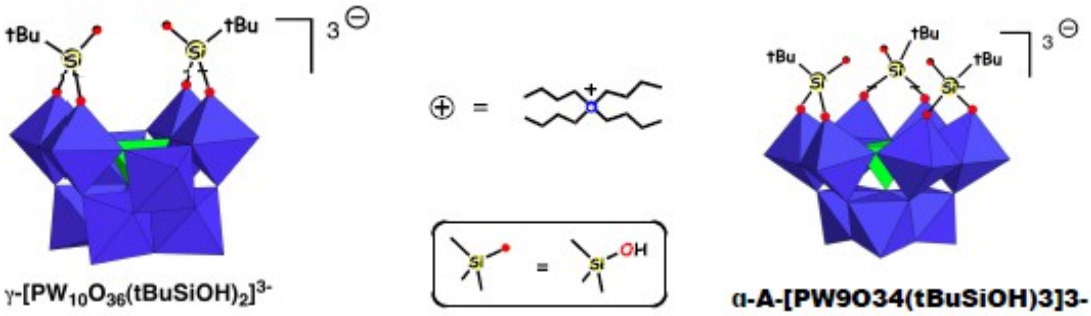

Fig. 27: $[TBA_3][PW_{10}O_{36}(tBuSiOH)_2]$ and $[TBA_3][PW_9O_{34}(tBuSiOH)_3]$

At the end of the reaction, the Cs^+ cation was exchanged with TBA^+, in order to increase solubility in polar organic solvents.

The products have been characterized *via* ^{1}H and ^{31}P NMR, on the basis of the singlet of ^{t}Bu at δ 1.1 ppm (for **PW10Si2**, Figure 28) and 1.0 ppm (for **PW9Si3**). The latter signal partially overlaps with the triplet of TBA. Nevertheless, its presence indicates that the reaction occurred successfully.

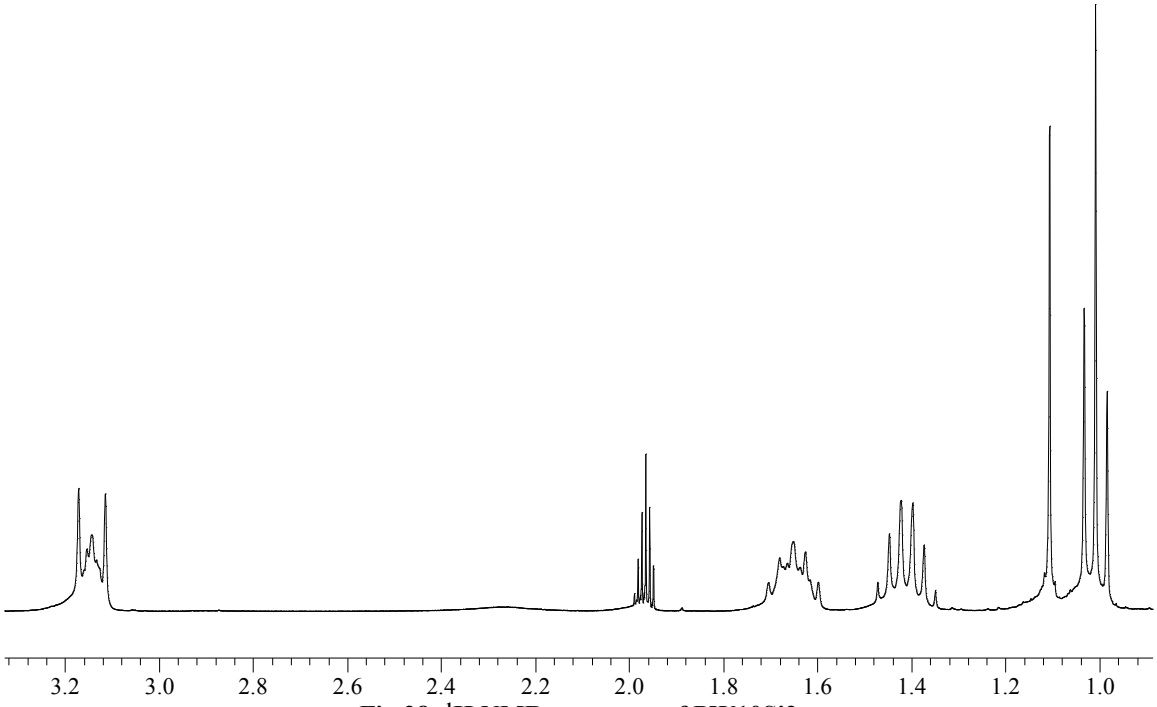

Fig.28: ^{1}H NMR spectrum of PW10Si2

^{31}P NMR spectra of both products gave a singlet, respectively at δ -14.9 ppm and -17 ppm, due to the unique phosphorus presents in the framework.

A further exchange of counter-ion was attempted, between Cs^{+} and didodecyldimethylammonium bromide ([DDA]Br), in order to obtain a species soluble in less polar solvents. Indeed, its TBA salt is only soluble in ACN, wich can react with hydrogen peroxide, under basic conditions, according to the following equation:

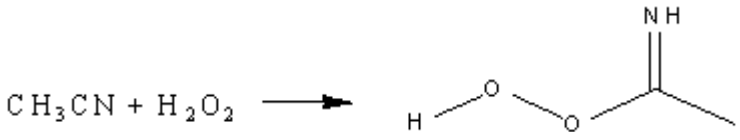

Thus, the exchange of counter-ion would have allowed the use of a less polar and unreactive solvent, such as toluene. However, impurities were found in the final product, and such strategy was discarded.

Subsequent POMs functionalization was carried out in order to obtain chemical species that can be used in catalytic and reactivity tests. For this purpose, early TMs, such as V^{V}, V^{III}, Ti^{IV} and Zr^{IV}, have been employed. POMs are "redox-active ligands", and the aim of this part of the work was to couple the redox properties of POMs with the catalytic properties of TMs.

3.2.2 POM(silanol) with early TMs for catalytic oxidation tests

The first synthesized species were those containing V^{V}-oxo group. Vanadium oxide is already known to be an active catalyst for oxidation reactions. For example, V_2O_5 is used in the oxidation of n-butanol to maleic anhydride.

Before each reaction with TMs, the POM was dried at 215°C under vacuum for 2 h. These conditions have been selected on the basis of previous TGA and NMR tests, which demonstrated that, in this way, H_2O was completely removed and the structure of the ligand preserved (Figure 29). It is very important to remove H_2O before the reaction in order to avoid hydrolysis of metal precursor and, subsequently, of silanol moieties grafted on the POM.

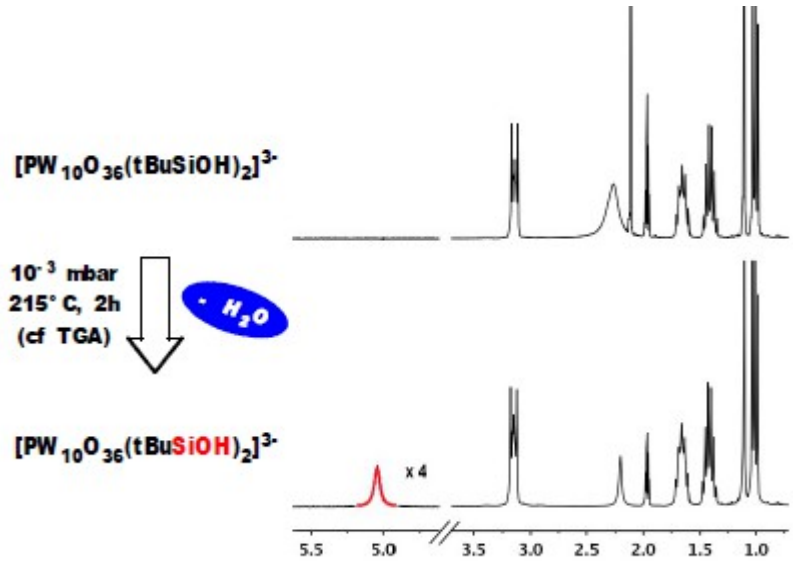

Fig. 29: NMR evolution of PW10Si2 after drying process

Following this procedure, **PW10Si2** was reacted with $V^{V}O(iPrO)_3$, resulting $[TBA]_3[PW_{10}O_{36}(tBuSiO)_2VO(iPrO)]$ (**PW10Si2VOPr**) (Figure 30).

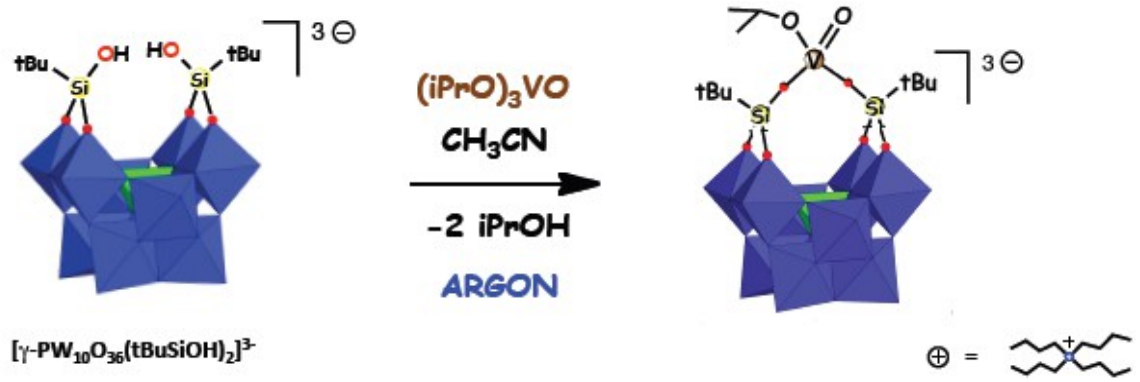

Fig. 30: Synthesis of PW10Si2VOPr

The compound was identified by ^{1}H NMR spectra, on the basis of the resonances of its ^{t}Bu (1.12 ppm) and ^{i}PrO (doublet at 1.50 ppm for the two equivalent methyl groups and multiplet at 5.66 ppm for the central C-H) groups (Figure 31):

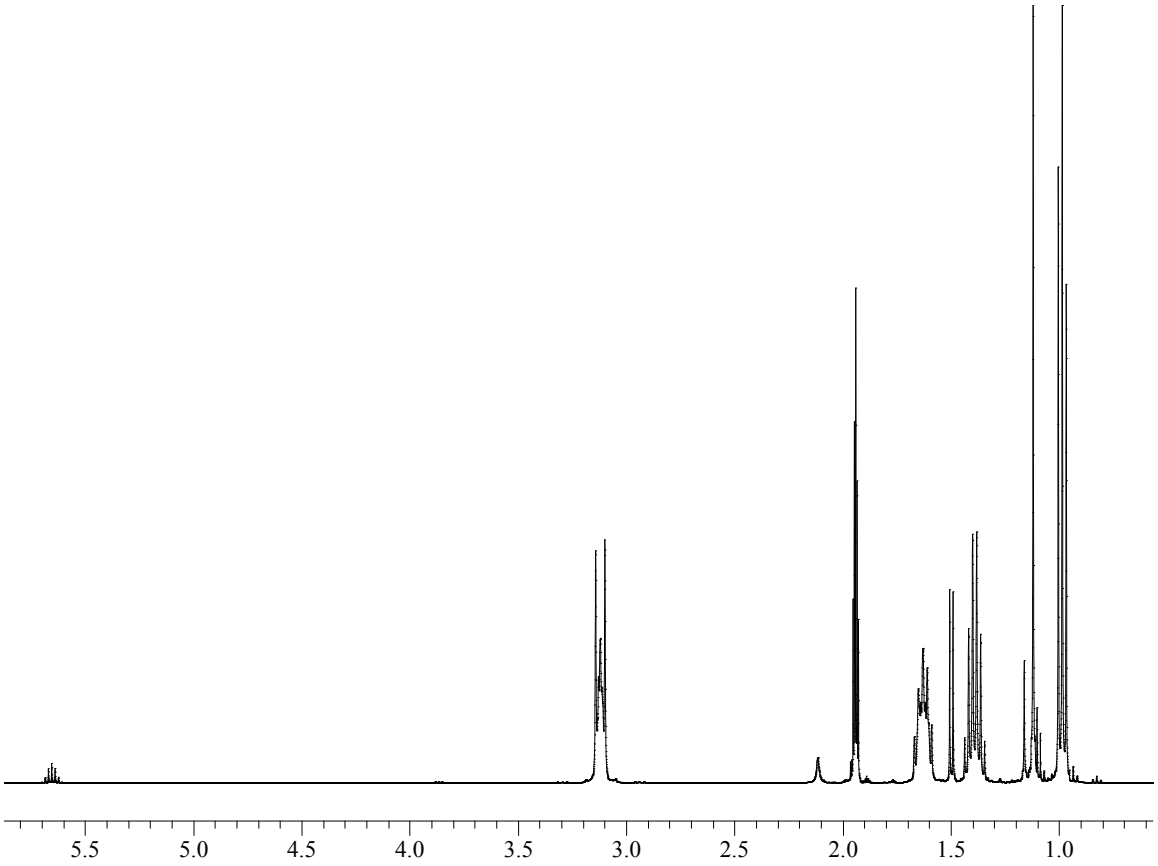

Fig. 31: ^{1}H NMR spectra of PW10Si2VOPr

Both ^{31}P and ^{51}V NMR spectra of **PW10Si2VOPr** display a singlet, at δ_P -14.50 ppm, and at δ_V -692 ppm. The presence of a minor impurity is also indicatedby a singlet at δ_V -722 ppm in the ^{51}V spectra.

Similarly, **PW9Si3** reacts with $VOCl_3$, to give $[TBA]_3[PW_9O_{34}(tBuSiO)_3VO]$ (**PW9Si3VO**)(Figure 32).

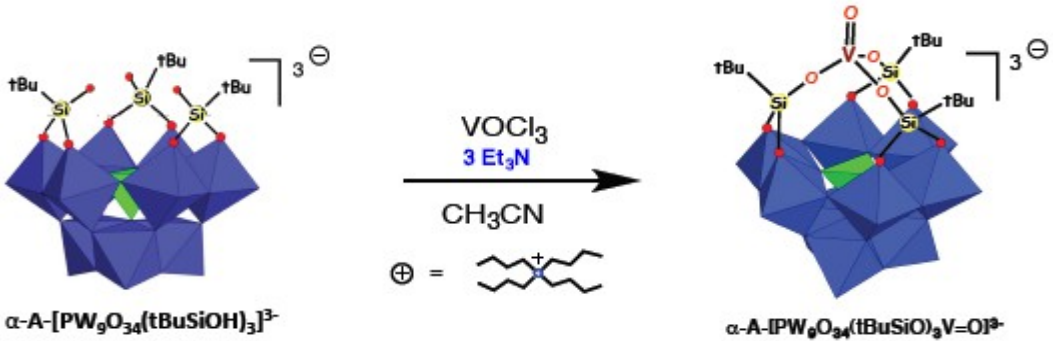

Fig. 32: Synthesis of PW9Si3VO

This hybrid, which synthesis is already known and studied[27], displays a completely saturated V, without possibility of further coordination. This fact is due in particular to the structural rigidity and the steric effects of the silanol groups This hybrids will be used as reference for the subsequent electrochemical analysis.

The complete conversion of **PW9Si3** into **PW9Si3VO** was determined by ^1H NMR, on the basis of the shift of the singlet of ^tBu from 1.00 to 1.20 ppm (Figure 33).

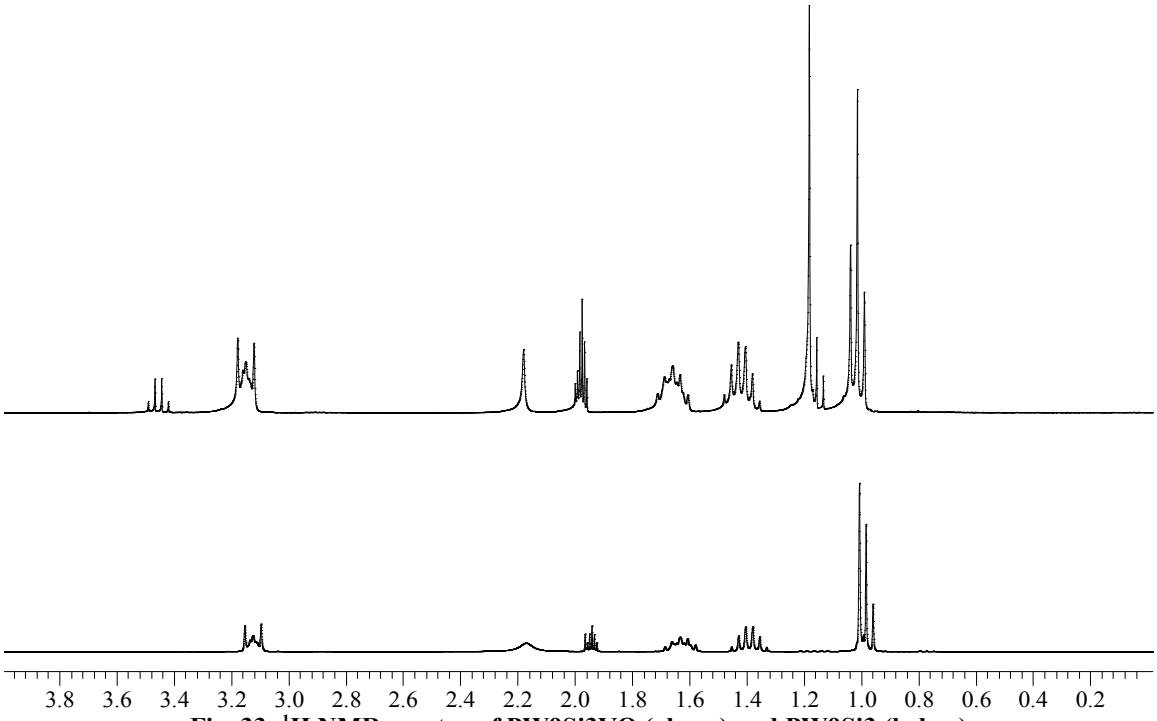

Fig. 33: ^{1}H NMR spectra of PW9Si3VO (above) and PW9Si3 (below)

The ^{31}P NMR spectra of **PW9Si3VO** shows a singlet at δ -15.60 ppm.

The utilization of oxygen donor molecules in the catalytic cycles could lead to detachment of vanadium centre from the POM, due to big oxofilicity of vanadium. This fact induced us to attempt the functionalization with metal atoms with a smaller oxofilicity. POM post-functionalization with Zr and Ti was carried out following the same procedure as above.

Thus, the reaction of **PW9Si3** with $ZrCl_4$ afforded $[TBA]_3[PW_9O_{34}(^tBuSiO)_3ZrCl]$ (**PW9Si3Zr**) (Figure 34).

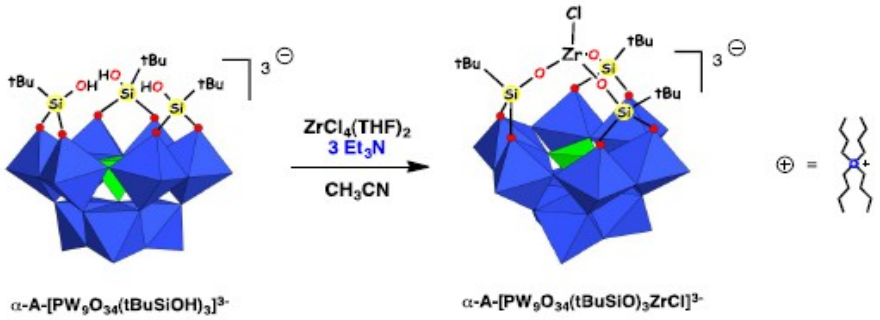

Fig. 34: Synthesis of PW9Si3Zr

Freshly distilled TEA was added in the reaction environment, to help the elimination of HCl, formed by the partial hydrolysis of $ZrCl_4$. The reaction evolution was monitored, on the ^1H NMR spectra, by the shift of the singlet of ^{t}Bu, from 1 to 1.2 ppm. However, the presence of several resonances between -10 and -20 ppm in the ^{31}P NMR spectrum (Figure 35) suggests the presence of impurities. Thus, purification was attempted by means of crystallization *via* diffusion of acetone on the ACN solution. The characterization of the product is now undergoing.

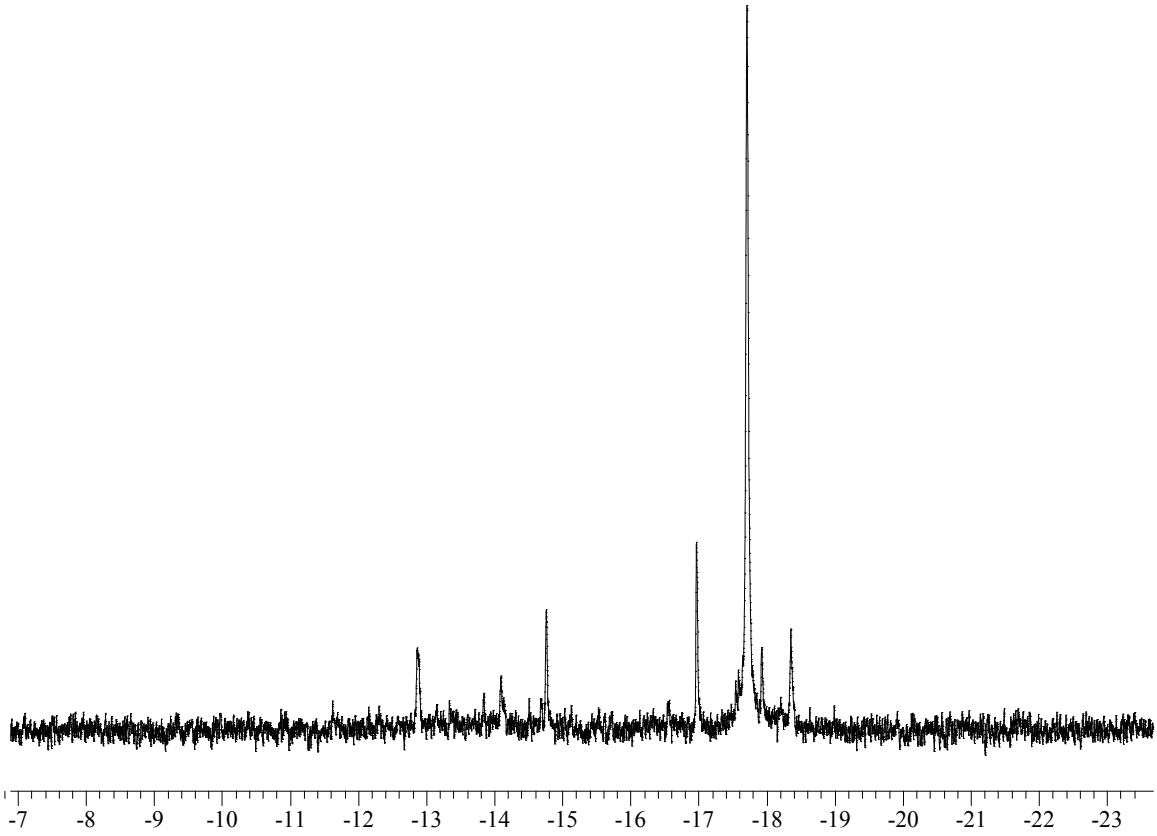

Fig. 35: ^{31}P NMR spectra of PW9Si3Zr

Finally, the reaction of **PW10Si2** with $Ti(^iPrO)_4$ resulted in a complex mixture of products, not yet identified.

3.2.3 Spectro-electrochemical analyses on POM-TM hybrids

In situ UV-Vis spectroelectrochemical analyses were carried out on POM-TM hybrids in order to study their redox behavior. In particular, the reduction of **PW9Si3** and **PW9Si3VO** was studied under Ar atmosphere. To individuate the reduction potentials of chosen hybrids, a CV test was carried out in advance. For the ligand **PW9Si3** the

potentials of -0.9 V and -1.3 V (vs. SCE) were measured; for the hybrid **PW9Si3VO** the potentials of -0.9 V and -1.7 V (vs. SCE) were measured.

A DFT modelization, carried out by Dr. Etienne Derat's team at the "*Institut Parisien de Chimie Moléculaire"* suggests that, for the compound **PW9Si3VO**, LUMO and LUMO+1, +2, +3 and +4 orbitals are centered on the tungstic framework. The spectro-electrochemical tests carried out in this Thesis have the aim to verify this analysis.

The test on **PW9Si3** was conducted in freshly distilled ACN containing POM $2x10^{-4}$ M, and every five minutes an UV-Vis spectrum was registered. The first electron reduction at -0.9 V (vs. SCE) was carried out for 65 minutes, until no change was identified in the UV-Vis spectra. The theoretical quantity of exchanged current was 0.59 C, while the effective exchanged current was 0.40 C. The second electron reduction was carried out at -1.3 V (vs. SCE), until no change was identified in the UV-Vis spectra. The first spectrum of the second series shows a fast increase at absorbance, perhaps due to the first residual reduction process. The second electrolysis took 45 minutes, for a theoretical exchange of 0.59 C and an effective exchange of 0.55 C. After that, a further electrolysis at -1.5 V (vs. SCE) was carried out, in order to terminate the second electron reduction. 0.25 C were exchanged, in 40 minutes. The total effective charge exchanged was 1.19 C, vs. a theoretical exchange of 1.20 C.

The test on **PW9Si3VO** was conducted in freshly distilled ACN, and every five minutes an UV-Vis spectrum was registered. The first electron reduction at -0.9 V (vs. SCE) was carried out for 90 minutes, until no change was identified in the UV-Vis spectra. The second electron reduction was carried out at -1.7 V (vs. SCE), for 90 minutes long.

The instrumentation assembling is here reported (figure 36):

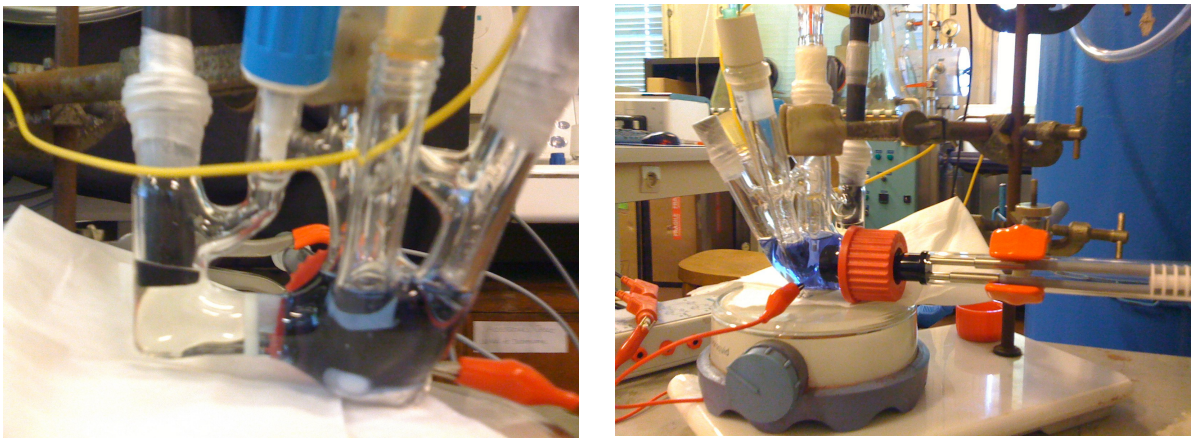

Fig. 36: Assembling of the spectro-electrochemical test on PW9Si3 and PW9Si3VO

The UV-Vis spectra recorded during the electrolysis of **PW9Si3** and **PW9Si3VO** are reported (Figure 37).

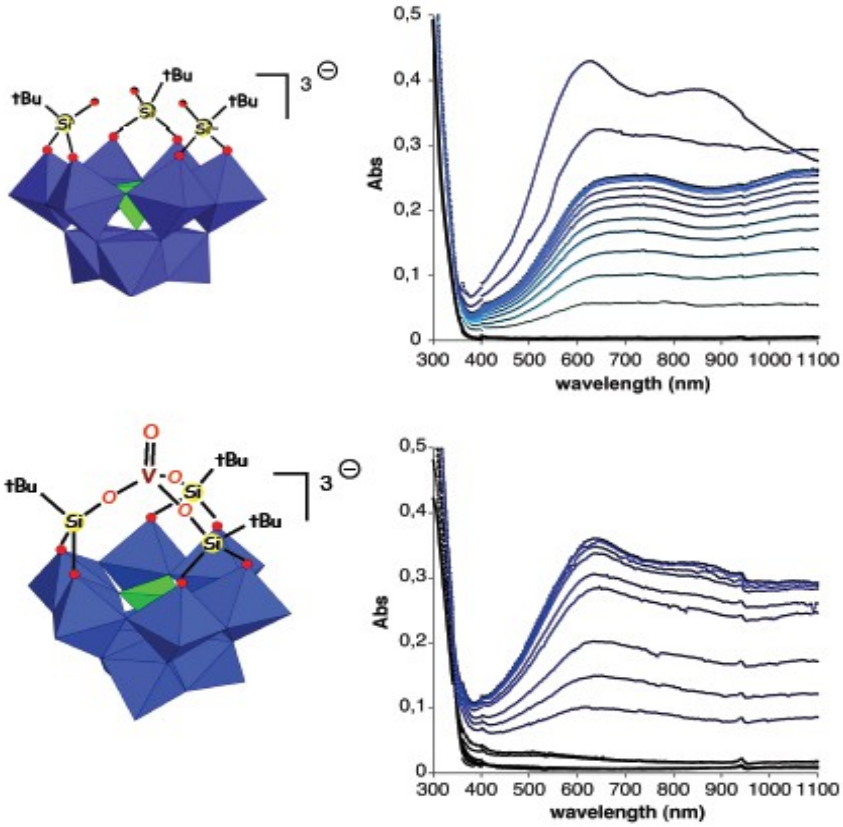

Fig. 37: Electro-UV analyses on PW9Si3 (top) and PW9Si3VO (down). Black profiles, first reduction; blue profiles, second reduction. ACN containing 0.1 M of $TBAPF_6$. Working electrode, Hg bed with Pt wire; reference electrode, SCE; counter-electrode, glassy carbon.

In both cases, the two reductions are mono-electronic. A strong blue color was observed after the first reduction, and the coloration persists also during the second reduction process.

The UV-Vis spectra of **PW9Si3VO** suggest a first reduction (black profiles) operated on the vanadium center ($V^{V} \rightarrow V^{IV}$). The second reduction (blue profiles) was centered on the POM framework ($W^{VI} \rightarrow W^{V}$) according to previous experiments and literature data.

EPR spectra were registered *ex situ* on the mono-reduced species (black line) and on the bi-reduced species after air reoxidation (red line) (Figure 38), in the case of **PW9Si3VO**.

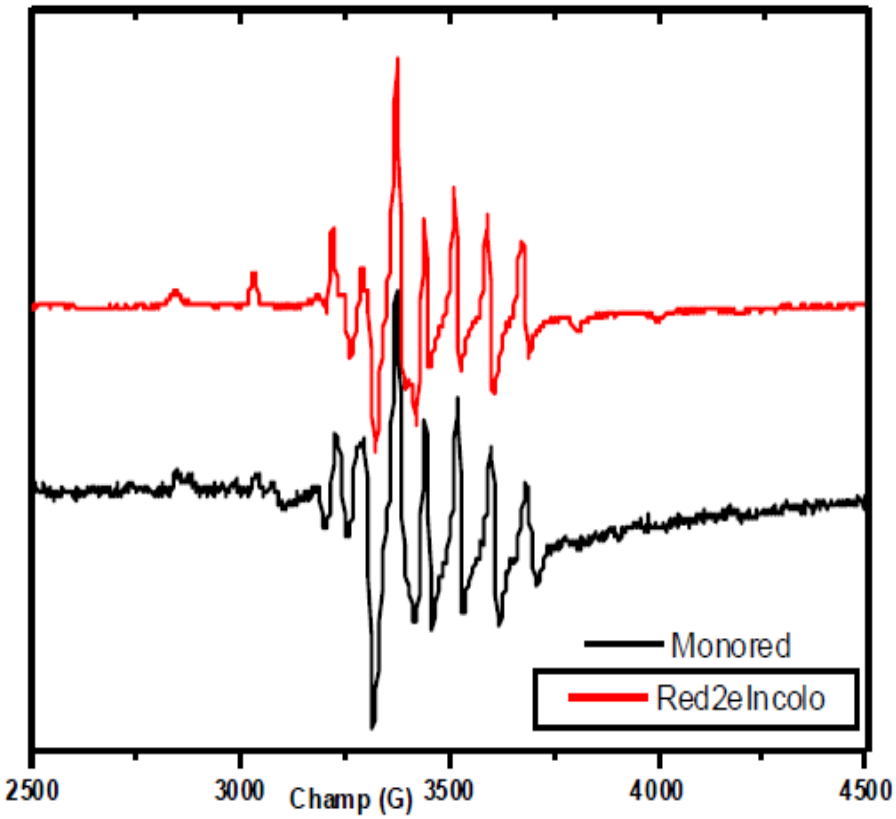

Fig. 38: EPR spectra on PW9Si3VO. Black line: monoreduction. Red line: bireduction after air reoxidation.

EPR spectra seem to agree with the presence of a paramagnetic V^{IV} species in both cases.

3.2.4 Catalytic oxidation tests on POM hybrids

Several catalytic oxidation tests were carried out, using the hybrids of POMs as catalysts. The oxidant agent was always tert-butylhydroperoxide (TBHP), whereas 3-methylbut-2-en-1-ol (ROH), an allylic alcohol, and 1-hexene have been employed as substrates (Figure 39). Vanadium species are already known to be active in olefins oxidation, such as cyclohexene.[28] An allylic alcohol was chosen because of the high affinity of vanadium for the alcohols in general; moreover, vanadium is known to be active in the oxidation of allylic alcohols.[29] The oxidation process concerns the epoxidation of the double bond of the substrate, and all the tests were carried out under Ar atmosphere.

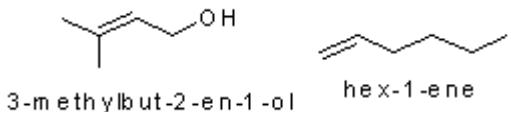

Fig. 39: The two selected substrates

The first test was carried out with 3% mol (as molar ratio) **PW10Si2VOPr** as catalyst, and the reaction monitored by ^{1}H, ^{31}P and ^{51}V NMR spectroscopy.

POM (9.14×10^{-3} M) and the olefin (0.3 M, 33 eq.) were added in the order to 0.5 mL of deuterated ACN. Through NMR analysis, the complete substitution of the ^{i}PrO ligand by the olefin was verified, thanks to the higher concentration of the latter. The olefin is supposed to bond the vanadium center with the terminal oxygen atom, thank to the high oxophilicity of vanadium. After that, TBHP was added, and the epoxide formation was monitored by ^{1}H NMR (Figure 40).

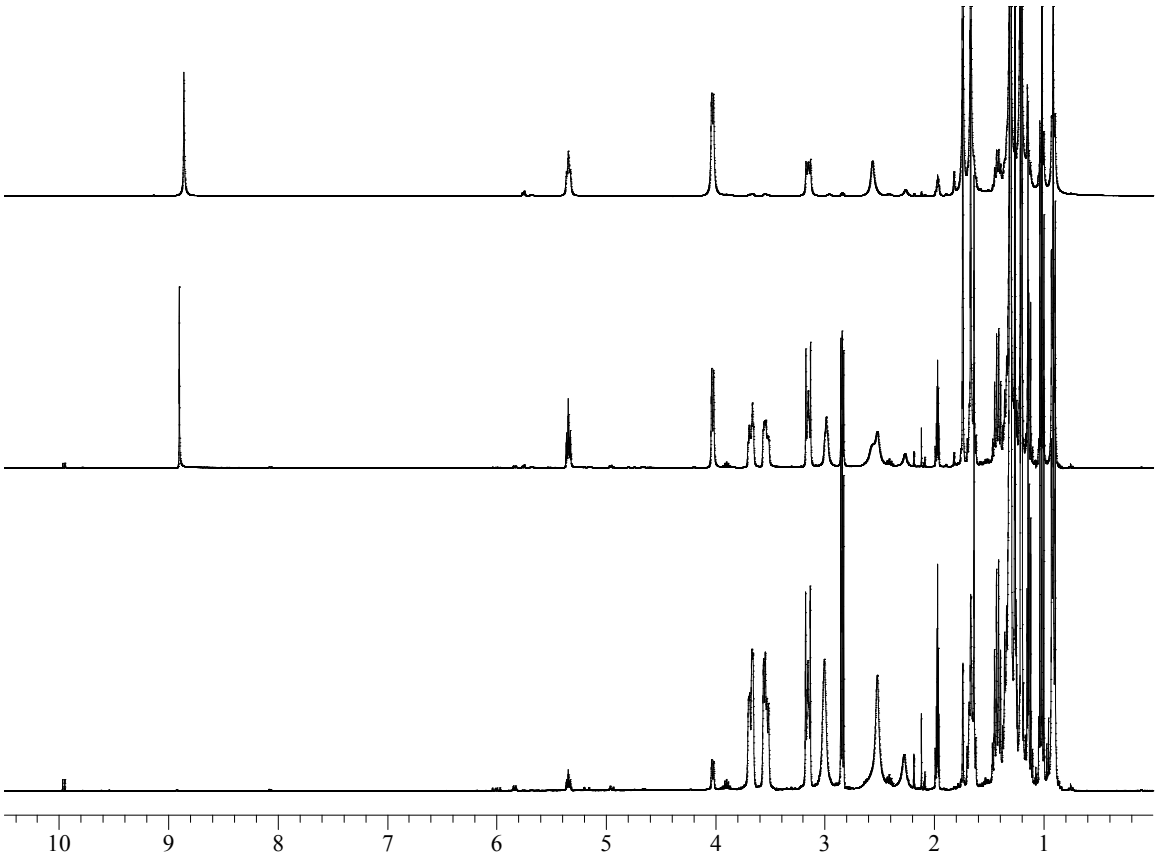

Fig. 40: ^{1}H NMR spectra recorded at different times during the oxidation of ROH with TBHP and 3% mol PW10Si2VOPr, in CD_3CN: top, after 6 min; centre, after 2h30; bottom, after 3 days

Observed resonances were those at 3.6 and 4 ppm, relative to the aliphatic CH_2 of respectively the final epoxide and the starting olefin. The conversion for the substitution of ^{i}PrO with ROH at the V centre is 95%, as calculated by integration of the ^{1}H NMR spectra. Therefore, the equilibrium constant for the substitution is 0.56. The iPrO (a secondary alcohol) group has a greater electron withdrawing effect than the olefine (a primary alcohol), and to move the equilibrium, a greater concentration of substrate respect to the catalyst was used.

Finally, the ^{51}V NMR spectrum of the final product shows a change in chemical shift compared to the starting material, which can be assigned to the expected predominant species, the ^{t}BuO-V.

Two other catalytic tests were carried out with **PW10Si2VOPr** as catalyst, varying its concentration respect to the previous one. POM was added at 0.1% mol and

0.01% mol (as molar ratio), to test its catalytic properties at different concentrations. The procedure was the same as above.

In the case of POM 0.1% mol, a catalytic activity was observed, while for the POM 0.01% mol an extremely few activity was observed after 7 hours.

In Table 1 and Table 2 the conversion vs. time results of the tests at 3% and 0.1% are reported:

Table 1:Test Catalyst 3% mol

t (min)	0	6	30	145	260	4320
Conv (%)	0	5	35	68	77	94

TON after 6 minutes: 1.7

TOF after 6 minutes: 0.3 min^{-1}

TON at 77% of conversion: 26

TOF at 77% of conversion: 0.1 min^{-1}

Final TON: 31

Final TOF: $7.25x10^{-3}$ min^{-1}

Table 2: Test Catalyst 0.1% mol

t (min)	0	60	195	240	330	405
Conv (%)	0	0	28	35	47	67

TON after 195 minutes: 278

TOF after 195 minutes: 1.42 min^{-1}

Average TON over 400 min: 670

Average TOF over 400 min: 1.65 min^{-1}

In the first test, TON and TOF were also calculated at 77% of conversion because of the long period elapsed between the beginning and the stop of the test. The calculated values of TOF indicate that the process with 0.1% mol of catalyst seems to be the most efficient. These results could indicate a possible deactivation or an interaction phenomena occurred to the catalyst at 3% of molar ratio, that can decrease its activity. Further studies have to be carried out, to confirm this supposition.

In Figure 41 the trends of conversion vs. time are reported:

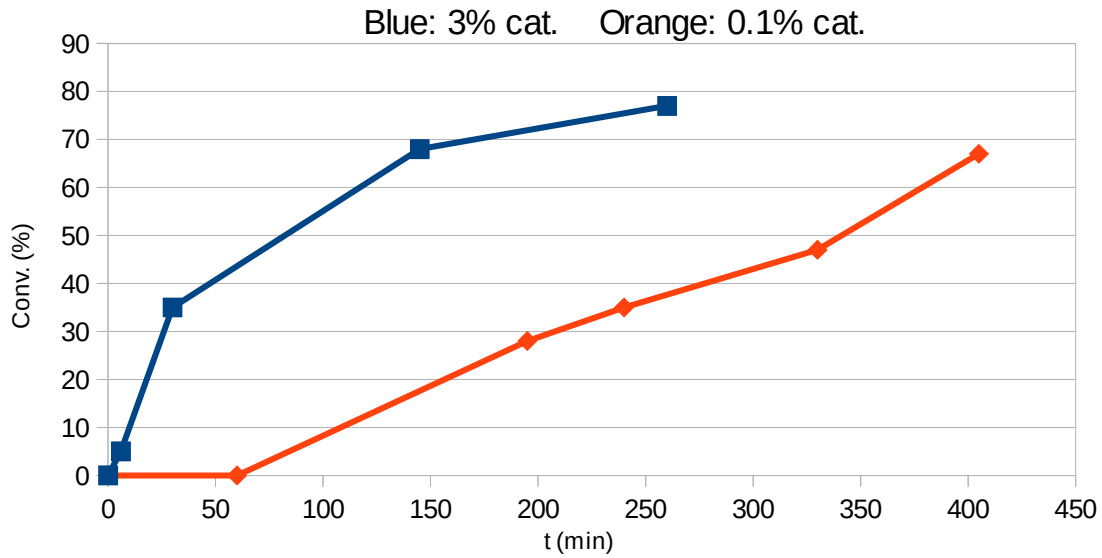

Fig. 41: Graphic Conv. vs time for the oxidation of ROH with TBHP, 3% and 0.1% mol catalyst

The limited number of data collected did not allow us to carry out kinetic studies, for which a larger number of data is needed.

A further test was carried out with 3% mol (as molar ratio) **PW9Si3VO** as catalyst. The reaction was monitored by ^{1}H, ^{31}P and ^{51}V NMR spectroscopy. POM ($9.14x10^{-3}$ M) and the olefin (0.3 M) were added in 0.5 mL of deuterated ACN. No reaction occurred at this stage, as shown by NMR analyses. This is due to the fact that the V-centre is fully saturated and not available for olefin coordination. Subsequently, TBHP was added to the reaction mixture, and, unexpectedly, epoxide formation was noticed, even if the conversion (determined by NMR) is not complete.

The unexpected catalytic effect may be due to catalysis operated by the POM framework, to a temporary detachment of the vanadium ion or to the presence of some impurities in the reaction environment. The study of this phenomenon will be the subject of the following tests.

The subsequent catalytic test was composed of two reactions, carried out at the same time. The two catalysts tested were **PW10Si2** and **PW9Si3**, which are not

functionalized POMs, and the tests were carried out to observe if they are able to catalyze the oxidation.

POMs (3% mol), 3 ml of freshly distilled ACN, the olefin (0.15 M) and TBHP (0.15 M) were added in this order in two separate Schlenk tubes, and the reaction was monitored by ^{1}H and ^{31}P NMR spectroscopy.

After approximately 20 h no formation of epoxide was observed, and the test was stopped. After this test, it was clear that POMs hybrids whitout vanadium centre are not able to catalyze the oxidation process.

To study the possible coordination of TBHP to different POMs, two further catalytic tests were carried out.

The first test was made on **PW10Si2VOPr,** (POM 3% mol, 0.5 ml of deuterated ACN and TBHP 0.3 M). The reaction was monitored by ^{1}H, ^{31}P and ^{51}V NMR spectroscopy. Formation of different products was observed. Three products were identified on the basis of ^{1}H and ^{51}V spectra: POM-V-^{i}PrO, POM-V-OO^{t}Bu and POM-V-O^{t}Bu. The presence of ^{t}BuOH was observed already in the starting product (^{t}BuOOH, 5.5 M in decane) used for the reaction, as evidenced by ^{1}H NMR analysis. This ^{t}BuOH is probably a result of the slow decomposition of the hydroperoxide.

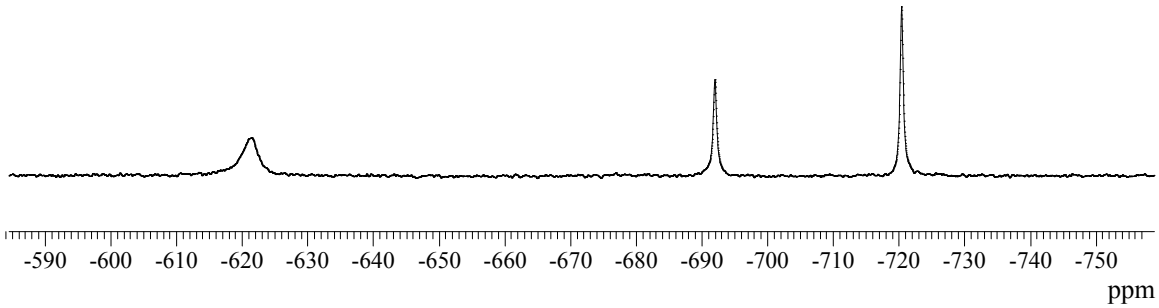

Fig. 42: ^{51}V NMR spectrum of the coordination of TBHP to PW10Si2VOPr. -690 ppm V-OiPr, -720 ppm V-OtBu and -620 ppm V-OOtBu

Then, the olefin (0.30 M) was added to the reaction mixture, and the reaction followed through NMR analyses. A unique ^{t}BuO(H) is coordinated to the V-centre and the formation of the epoxide is quantitative. In this way, it was possible to conclude that the catalytic process works also by inverting the order of addition of the reagents.

Another test, using only ^{t}BuOOH, was carried out with **PW9Si3VO** as catalyst. POM (3% mol as molar ratio) in 0.5 mL of deuterated ACN and ^{t}BuOOH (0.30 M) were added in the order in an NMR tube. The NMR analyses, carried out after 1 h 30 min, did not show any change in the solution composition. In this way, it was possible to conclude that the vanadium does not separate from the POM framework during the reaction. Therefore, unexpected catalytic activity of **PW9Si3VO** is therefore probably due to the presence of impurities in the starting material.

The catalytic properties of **$VO(iPrO)_3$** were also tested. $VO(iPrO)_3$ (3% mol), 0.5 mL of deuterated ACN and the olefin (0.3 M) were added in an NMR tube. ^{1}H and ^{51}V NMR analyses were performed, and then TBHP 0.3 M was finally added. ^{1}H and ^{51}V NMR analyses were carried out after 25 minutes (87% of conversion), after 1 hour and 25 minutes (96% of conversion) and after 2 hours and 50 minutes (*ca.* 100% of conversion). It can be concluded that **$VO(iPrO)_3$** results in a greater reaction rate than POM-V. Neverthless, as indicated by NMR, several V-containing species are present at the end of the reaction (Figure 43).

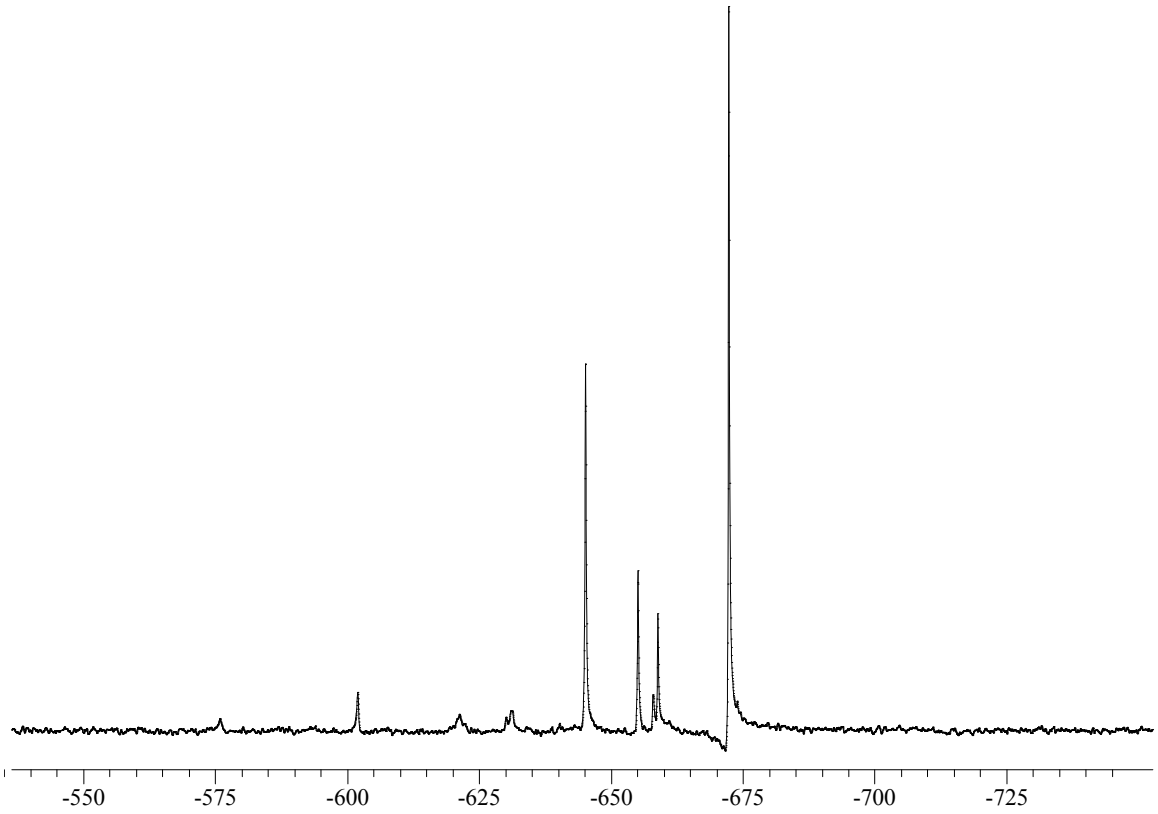

Fig. 43: ^{51}V NMR spectra at the end of the oxidation of ROH with TBHP, with $VO(iPrO)_3$ as catalyst.

Finally, we performed some catalytic tests using 1-hexene, instead of 3-methylbut-2-en-1-ol. **PW10Si2OPr** (3% mol), 3 mL of freshly distilled ACN, 1-hexene 0.15 M and TBHP (0.15 M) were added in a Schlenk tube.

The reaction was monitored *via* ^{1}H NMR. After 6 h of reaction, epoxide formation was not observed, and the reaction was discarded. The unsuccessful coordination is due to the lack of terminal oxygen atoms on the hexene molecule. This fact does not allow the coordination to the vanadium center, preventing the subsequent oxidation of the double bond.

The proposed mechanism for the epoxidation is the one reported in literature, for the epoxidation operated by V^{V} species (Figure 44). In our case, the OR groups bonded to the vanadium center are represented by the POM-Si framework.

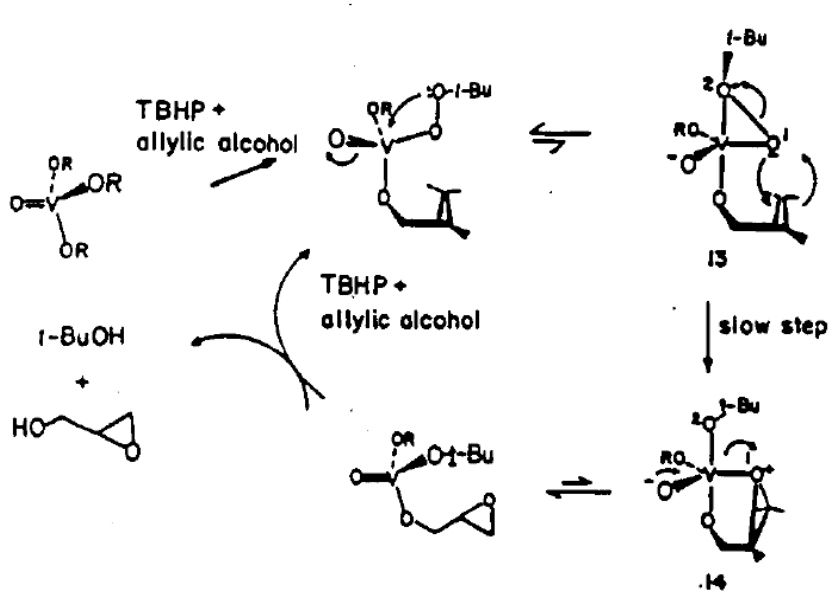

Fig. 44: Mechanism of epoxidation operated by V^{V} species[viii]

3.2.5 POM(silanol) with V^{III} for reactivity tests

The functionalization attempted with V^{III} is the reaction between $VCl_3(THF)_3$ and **PW9Si3**, to give $[TBA]_3[PW_9O_{34}(tBuSiO)_3V]$ (**PW9Si3V**) (Figure 45).

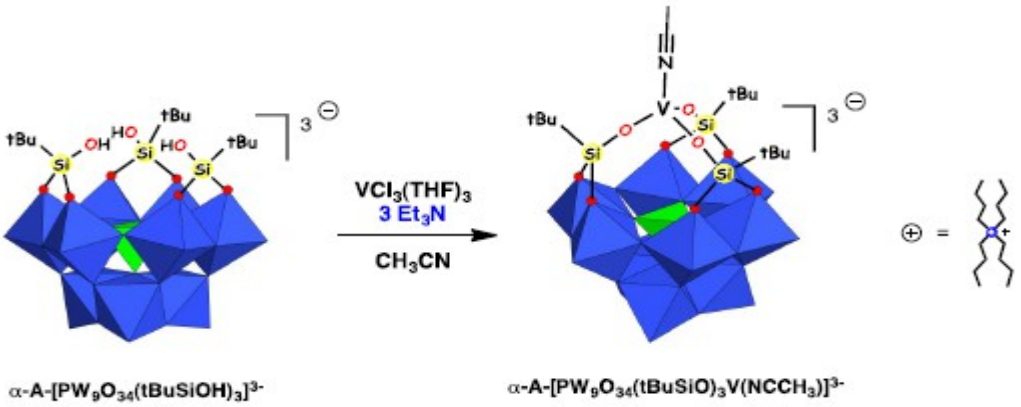

Fig. 45: Synthesis of PW9Si3V

Freshly distilled TEA was added in the reaction environment, to help the elimination of HCl, formed by the partial hydrolysis of VCl_3. As soon as VCl_3 was added to the reaction mixture, in the presence of TEA, formation of a dark blue solution was observed. This indicates the presence of reduced forms of POM, as a result of an inner sphere electron transfer from the metal to the POM framework of at least one electron, resulting in the formation of a V^{IV} species, or two electrons along the oxidation of vanadium to +5 oxidation state. The nature of the occurred process will be investigated with spectro-electrochemical analyses. This reaction allowed obtaining a hybrid where vanadium is in an intermediate oxidation state. The presence of d electrons on the metal center allows to carry out reactivity studies with small molecules.

The reaction was monitored by ^1H NMR, following the shift of the singlet of -tBu from 1.04 to 0.97 ppm. The presence of broad signals suggests the formation of paramagnetic species.

Two UV-Vis analyses were also carried out on the reaction product. A spectrum was registered directly on the crude product (Figure 46), and it shows the features of a mono-electronic oxidation occurred on vanadium ($V^{III} \rightarrow V^{IV}$) ($\lambda_{max}$ = 400 nm) and a mono-electronic reduction occurred on tungsten ($W^{VI} \rightarrow W^{V}$) (λ_{max} = 900 nm) of the POM framework (see paragraph 3.2.3 "Spectro-electrochemical analyses on POM-TM hybrids").

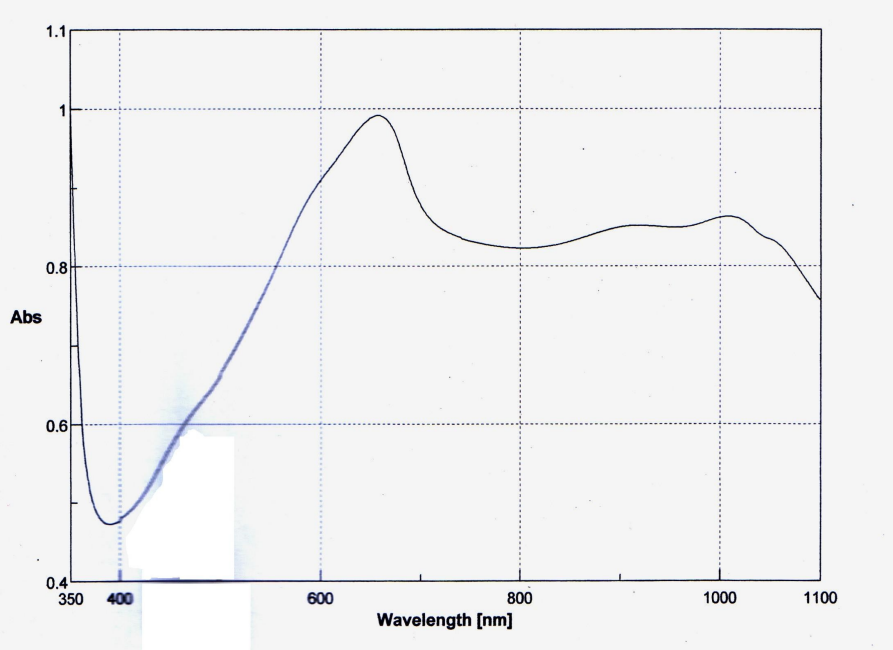

Fig. 46: UV-Vis spectra of crude PW9Si3V

The second UV-Vis spectrum was registered on the dried and purified product (Figure 47), and shows a weak absorbance, that probably indicates the presence of a V^{IV} centre. This can indicate the reoxidation of the W centre of POM, occurred during the drying processes, and the instability of the reduced state of the W.

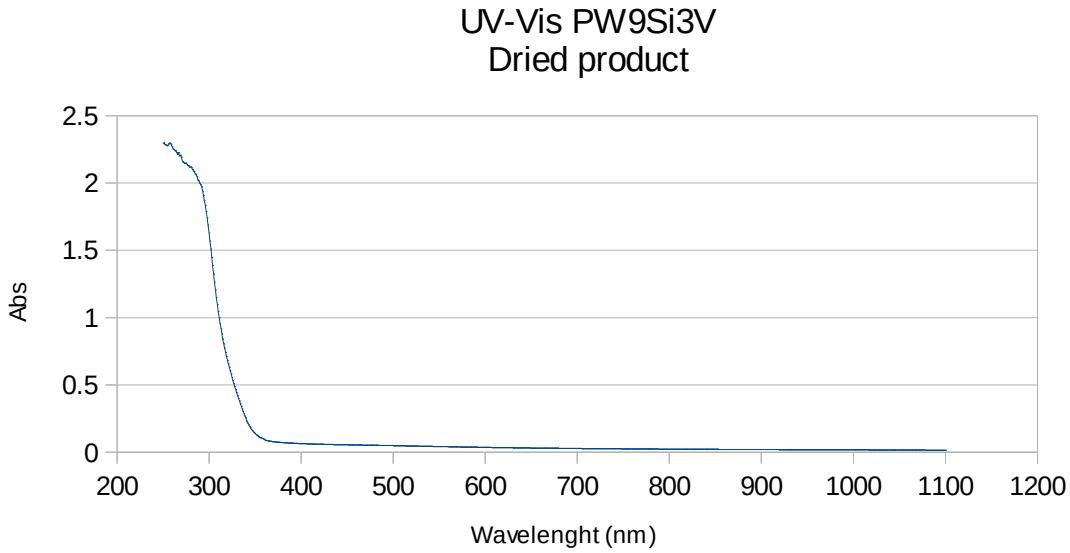

Fig. 47: UV-Vis spectra of dried PW9Si3V

The first reactivity test was carried out between **PW9Si3V** and styrene oxide. The reaction was supposed to yield styrene and POM-VO, as indicated by ^{1}H, ^{31}P and ^{51}V NMR spectroscopy.

The conversion was calculated by integration of the ^{1}H NMR spectra (Figure 48), observing multiplets at 2.8 ppm and at 5.3 ppm, relative respectively to one methylenic proton of the oxyrane ring of styrene oxide and to the same proton of styrene. The result was a conversion of styrene oxide into styrene of 40%.

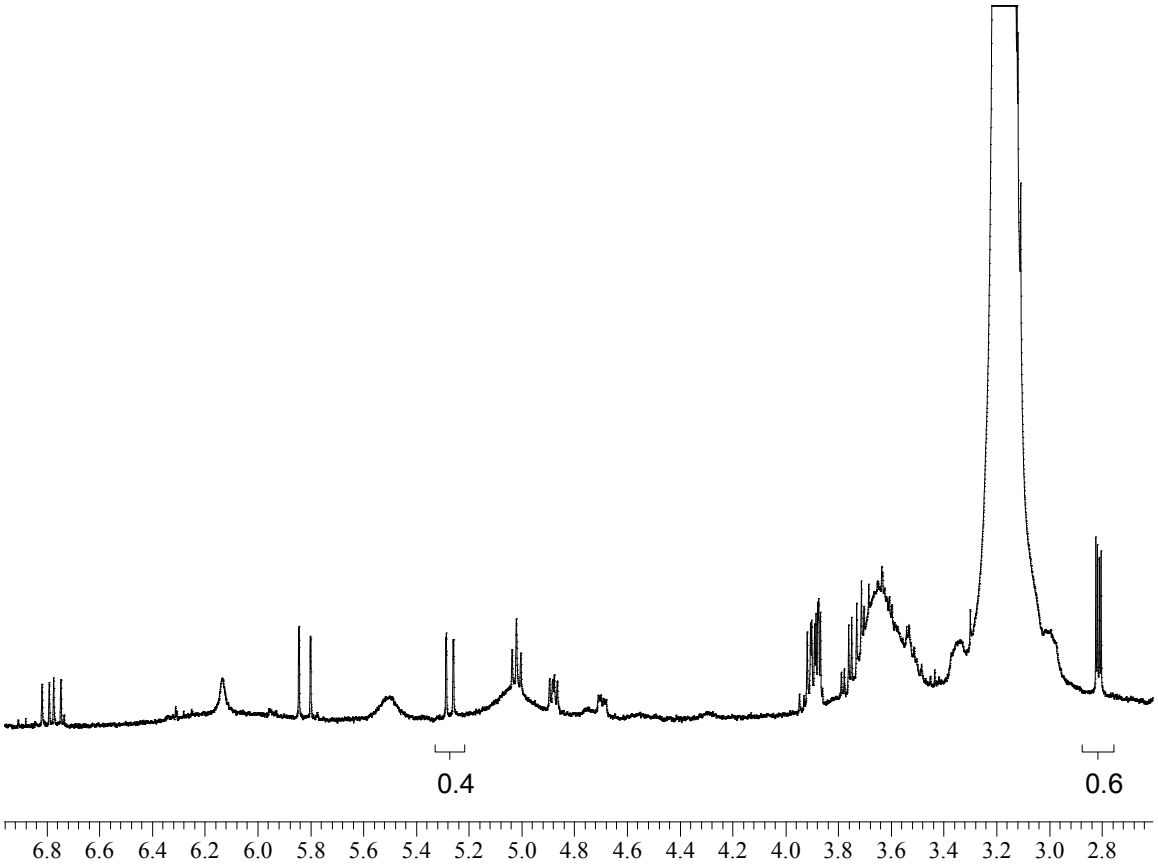

Fig. 48: ^{1}H NMR spectra of the reaction between PW9Si3V and styrene oxide. Final rate betwwen styrene (0.4) and styrene oxide (0.6) is calculated.

In the ^{51}V NMR spectrum, the resonance of $V^{V}O$ was recognized, at -800 ppm, with several other resonances, attributable to the starting product and other by-products. This means that the desired reaction took place, but the conversion was not complete.

The second test carried out was the reaction between **PW9Si3V** and ethyl-2-diazoacetate (diazo). The analyses carried out for the moment on the crude product did not allow to understand the products evolution. The ^{1}H NMR spectrum shows the

resonances of the starting products, and IR analysis will be necessary in the future to establish the eventual bond between the vanadium and the diazo FG. It can be observed with the shift of the absorption band of the diazo double bond N=N.

4. CONCLUSIONS

During this Thesis, several reactions and tests have been carried out, in order to couple the redox properties of POMs with the chemical properties of several FGs.

In the field of photochemical processes, several hybrids were obtained and their redox properties investigated. After that, other electrochemical tests were carried out on the compounds at Jena University. Luminescence tests carried out on **K_{Sn}^{W}[IrOxa]** and **K_{Sn}^{Mo}[IrOxa]** revealed, for the former, a strong luminescence phenomenon, while for the latter a weak luminescence phenomenon. For **K_{sn}^{Mo}[IrOxa]**, the luminescence is quenched by an electron transfer from the iridium chromophore to the POM, and this effect can be used in the future for hydrogen photoproduction. Charge photoaccumulation and hydrogen photoproduction on **K_{sn}^{Mo}[IrOxa]** are at the moment under investigation.

On the other hand, also pyridinic photoactive POMs were synthesized. **D_{Si}^{W}[Pyr]$_2$** and **K_{Sn}^{W}[Pyr]** were obtained and their redox properties analyzed. These compounds will be used, in the future, for the polymerization of photoactive films.

For POM applications in catalysis and reactivity tests, firstly a functionalization with silanol moieties was carried out. This strategy allowed to obtain POM hybrids that mimic the silica surfaces already developed in heterogeneous catalysis, but on a homogeneous catalyst. Metal complexes were prepared with early TMs such as V^{V}, Ti^{IV}, Zr^{IV} and V^{III}.

The redox properties of POM-V^{V} hybrids were studied by spectro-electrochemical and EPR techniques. The electrolysis process revealed two monoelectronic reductions, UV-Vis analyses suggest that the first reduction is probably centered on the vanadium atom ($V^{V}\rightarrow V^{IV}$) and the second reduction is centered on the tungstic POM framework ($W^{VI}\rightarrow W^{V}$). The EPR spectrum registered on the monoreducted species suggests the probable presence of a V^{IV} centre.

The subsequent epoxidation tests were carried out with POM-V^{V} hybrids as catalysts, TBHP as oxidant and 3-methylbut-2-en-1-ol as substrate. The best TOF value was obtained with 0.1% mol **PW10Si2OPr** as catalyst. It was also observed that the reagent addition order does not affect the outcome of the test. A test was also carried out

with 1-hexene as substrate, but it did not undergo epoxidation, because of the lack of reactivity of such systems for unfunctionalized olefins. A final test was carried out with **$VO(iPrO)_3$** as catalyst. As expected, it led to the epoxidate allylic alcohol, but the catalyst turned out to be not recoverable from the reaction environment. Conversely, the coordination of vanadium to the POM framework allows the recovery of the catalyst, because of the formation of only one or two main species that can be reconverted back to the starting product. Furthermore, the POM-V hybrid can stabilize the precatalytic species.

A POM-V^{III} hybrid was used in reactivity tests with small molecules. It is supposed to accomplish an electron donation, thanks to the d-electrons present on vanadium center, and in this way to activate small molecules. Reactivity of **PW9Si3V** was tested with styrene oxide and ethyl-2-diazoacetate (diazo). In the case of styrene oxide the formation of styrene and a POM-V^{V} species was observed, while for the reaction with the diazo compound further spectrochemical analyses will be necessary.

5. EXPERIMENTAL SECTION

General methods

Microwawe assisted syntheses were performed at ambient pressure in a Milestone Start S. reactor, equipped with a temperature control unit (operating conditions around 40 W). The ^{1}H, ^{31}P and ^{51}V NMR spectra were recorded at room temperature in 5 mm. o.d. tubes, with an Advance Bruker 300 and Advance Bruker 400 MHz. The UV-Vis spectra were recorded with a Jasco V530 spectrometer, without Peltier Module. The electrochemical analyses were recorded with an Autolab PGSTAT 100 instrument. The X-Band EPR spectra were recorded with a Bruker Elexsys 500 with Oxford Instrument continuous-flow liquid-helium cryostat and a temperature control system. The cyclovoltammetric analysis of the products for photochemical applications were conducted in DMF containing 0.1 M of $TBAPF_6$. Working electrode, glassy carbon; reference electrode, SCE; counter-electrode, Pt wire. The cyclovoltammetric analysis of the products for catalytic applications were conducted in ACN containing 0.1 M of $TBAPF_6$. Working electrode, Pt wire; reference electrode, SCE; counter-electrode, glassy carbon. The electrolysis tests were conducted in ACN containing 0.1 M of $TBAPF_6$. Working electrode, Hg bed with Pt wire; reference electrode, SCE; counter-electrode, glassy carbon. The scan rate of all cyclovoltammetric analysis was 0.1 V/s.

5.1 POST-FUNCTIONALIZATION OF POMs FOR PHOTOCHEMICAL APPLICATIONS

5.1.1 Synthesis of $[TBA]_6[P_2W_{17}O_{62}(Si\text{-}C_6H_4\text{-}ethynylPyr)_2]$ ($D_{si}^{W}[Pyr]_2$)

A mixture of $\mathbf{D_{si}^{W}[I]}$ (400 mg, $6.56x10^{-5}$ mol), 1-ethynylpyrydine (**Pyr**) (50 mg, $3.51x10^{-4}$ mol), CuI (1.6 mg, $8.40x10^{-6}$ mol) and $Pd(PPh_3)_2Cl_2$ (8 mg, $1.14x10^{-5}$ mol) was prepared in a Schlenk tube under Ar atmosphere. 6 mL of pure and fresh DMF were then added, under Ar atmosphere. After careful degassing with argon for 5 minutes, 280 mg ($2.77x10^{-3}$ mol) of freshly distilled TEA were added. The mixture was stirred at 80°C for 1h, under microwawe irradiation. After cooling at room temperature, the obtained solution was precipitated with diethyl ether, centrifuged and filtered. The solid was extracted with a solution of [TBA]Br in DCM, washed twice with water and the organic phase was collected and concentrated up to ca. 10 mL. Three drops of TEA were added in order to

eliminate acidity and the product precipitated by addition of diethyl ether. A white-grey solid was obtained after filtration. To eliminate the excess of TEA, the solid was collected and a mixture of [TBA]Br and DCM was added. The solution was washed four times with distilled water, and the organic phase was collected and precipitated with diethyl ether. The solid was filtered and collected. Yield: 177 mg, 45%.

^{1}H NMR (CD_3CN): δ 1.00 (t, 72H), 1.41 (m, 48H), 1.63 (m, 48H), 3.15 (m, 48H), 7.48 (m, 4H), 7.63 (d, 4H), 7.92 (d, 4H), 8.61 (m, 4H)

5.1.2 Synthesis of $[BMIM]_3[PW_{11}O_{39}Sn(p\text{-}C_6H_4\text{-ethynyl-IrOxazole})]$ (K_{Sn}^{W} [IrOxa])

A mixture of $\mathbf{K_{Sn}^{W}[I]}$ (100 mg, 2.52×10^{-5} mol), ethynyl-IrOxazole (**IrOxa**) (42.5 mg, 4.41×10^{-5} mol, 1.75 eq.), CuI (0.4 mg, 2.10×10^{-6} mol) and $Pd(PPh_3)_2Cl_2$ (1.6 mg, 2.29×10^{-6} mol) was prepared in a Schlenk tube under Ar atmosphere. 4 mL of pure and fresh DMF were added, under Ar atmosphere. After careful degassing with argon for 5 minutes, 100 mg (9.90×10^{-4} mol) of freshly distilled TEA were added, and the solution changed its colour, from orange to red. The mixture was stirred at 80°C for 1h, under microwawe irradiation. After cooling at room temperature, the obtained solution was precipitated with diethyl ether, and the precipitate filtered. The obtained solid wash washed with ethanol, to remove the excess of Ir complex. The solid was filtered and dissolved in the minimal amount of DMSO. $BMIM^+Cl^-$ (ionic liquid) was added, to exchange the counter-ion, and ethanol was added to allow precipitation of the product. The solid was filtered. To remove the excess of BMIM and impurities, the solid was dissolved again in the minimal DMSO necessary, and a double volume of ACN was added to allow the impurities to precipitate. The obtained solution was precipitated with diethyl ether, and the solid was collected and filtered. Yield: 72 mg, 65%.

^{1}H NMR (D_6-DMSO): δ 0.90 (t, 9H), 1.28 (m, 6H), 1.78 (m, 6H), 3.86 (s, 9H), 4.16 (t, 6H), 6.25-9.25 (m, 26H)

5.1.3 Synthesis of $[BMIM]_3[PMo_{11}O_{39}Sn(p\text{-}C_6H_4\text{-ethynyl-IrOxazole})]$ (K_{Sn}^{Mo}[IrOxa])

A mixture of $\mathbf{K_{Sn}^{Mo}[I]}$ (100 mg, 3.33×10^{-5} mol), ethynyl-IrOxazole (**IrOxa**) (56.3 mg, 5.83×10^{-5} mol, 1.75 eq.), CuI (0.5 mg, 2.78×10^{-6} mol) and $Pd(PPh_3)_2Cl_2$ (2.2 mg, 3.03×10^{-6} mol) was prepared in a Schlenk tube under Ar atmosphere. 4 mL of pure and fresh DMF were added, under Ar atmosphere. After careful degassing with argon for 5 minutes, 100 mg (9.90×10^{-4} mol) of freshly distilled TEA were added, and the solution changed its

colour, from orange to red. The mixture was stirred at 80°C for 1h, under microwawe irradiation. After cooling at room temperature, the obtained solution was precipitated with diethyl ether, and the precipitate filtered. The solid was dissolved in the minimal quantity of DMSO, and the insoluble part was filtered. A quantity of $BMIM^+Cl^-$ (ionic liquid) was added, to exchange the counter-ion, and ethanol was added to allow precipitation of the product. The solid was filtered. To eliminate the impurities, the solid was dissolved in the double of the minimal quantity of ACN needed, and stirred for four hours. The product, present in the solution, was precipitated with diethyl ether, and the solid obtained was filtered. Yield: 42 mg, 37%. ^{1}H NMR (CD_3CN): δ 0.90 (t, 9H), 1.28 (m, 6H), 1.78 (m, 6H), 3.86 (s, 9H), 4.16 (t, 6H), 6.25-9.25 (m, 26H)

^{31}P NMR (CD_3CN): δ -2.93 (s, 1P)

5.1.4 Synthesis of $[TBA]_3[PW_{11}O_{40}(Si\text{-}C_6H_4\text{-}ethynylPyr)_2]$ ($K_{Si}^W[Pyr]_2$)

A mixture of $\mathbf{K_{Si}^W[I]}$ (400 mg, $1.03x10^{-4}$ mol), 1-ethynylpyrydine (**Pyr**) (86 mg, $6.18x10^{-4}$ mol), CuI (1.6 mg, $8.24x10^{-6}$ mol) and $Pd(PPh_3)_2Cl_2$ (11 mg, $1.55x10^{-5}$ mol) was prepared in a Schlenk tube under Ar atmosphere. 9 mL of pure and fresh DMF were added, under Ar atmosphere. After careful degassing with argon for 5 minutes, 280 mg ($2.77x10^{-3}$ mol) of freshly distilled TEA were added. The mixture was stirred at 80°C for 1h, under microwawe irradiation. After cooling at room temperature, 0.7 g of TBABr were added, the obtained solution was precipitated with diethyl ether, and the precipitate filtered. A dark green gel was obtained. The compound was dissolved in the minimal amount of ACN, and 0.5 g of TBABr and 0.5 g of EDTA were added to increase the solubility of the product. The insoluble residue was filtered off and the dark orange solution containing the final product was precipitated by addition of absolute ethanol. The solid was filtered and collected, and then dissolved with 10 ml of ACN. The insoluble part was filtered, and the liquid part was concentrated up to few drops. The product, still dissolved in ACN, was precipitated with diethyl ether, and the obtained solid was filtered and collected. Yield: 131.20 g, 33%.

^{1}H NMR (CD_3CN): δ 1.00 (t, 36H), 1.41 (m, 24H), 1.63 (m, 24H), 3.15 (m, 24H), 7.48 (m, 4H), 7.70 (d, 4H), 7.92 (d, 4H), 8.61 (m, 4H)

^{31}P NMR (CD_3CN): δ -13.25 (s, 1P)

5.2 FUNCTIONALIZATION OF POMs FOR REACTIVITY TESTS AND CATALYTIC APPLICATIONS

5.2.1 Synthesis of $[TBA]_3[PW_{10}O_{36}(^tBuSiOH)_2]$ (PW10Si2)

5 g ($1.48x10^{-3}$ mol) of $Cs_7[PW_{10}O_{36}]$ were introduced in a Schlenk tube, under argon atmosphere. 50 mL of freshly distilled ACN were added, under argon atmosphere, and the Schlenk tube was cooled at 0°C for 10 min. $^tBuSiCl_3$ (0.851 g, $4.44x10^{-3}$ mol) and [TBA]Br (1.910 g, $5.92x10^{-3}$ mol) were added and the solution stirred at 0°C overnight, under argon atmosphere. The day after, the withe solid formed was filtered (essentially CsBr + CsCl) and the product was then crystallized at room temperature, in an open vessel. After three hour, the first crystals formed were eliminated, and the resulting solution again crystallized for one day. The latter crystals formed were washed with diethyl ether and collected. Yield: 2.985 g, 60%

^{1}H NMR (CD_3CN): δ 1.00 (t, 36 H), 1.10 (s, 18 H), 1.41 (m, 24 H), 1.65 (m, 24 H), 3.15 (m, 24 H)

^{31}P NMR (CD_3CN): δ -14.90 (s, 1 P)

5.2.2 Synthesis of $[TBA]_3[PW_9O_{34}(^tBuSiOH)_3]$ (PW9Si3)

3 g ($1.05x10^{-3}$ mol) of $K_9[PW_9O_{34}]$ were introduced in a Schlenk tube under argon atmosphere. 30 mL of freshly distilled ACN were added, under argon atmosphere, and the Schlenk tube was cooled at 0°C for 10 min. $^tBuSiCl_3$ (0.601 g, $3.14x10^{-3}$ mol) and [TBA]Br (1.350 g, $4.20x10^{-3}$ mol) were added and the solution stirred at 0°C overnight, under argon atmosphere. The day after, the withe solid formed was filtered (essentially CsBr + CsCl) and the product was then crystallized at room temperature, in an open vessel. After three hours, the first crystals formed were eliminated, and the resulting solution again crystallized for one day. The latter crystals formed were washed with diethyl ether and collected. Yield: 0.464 g, 12%

^{1}H NMR (CD_3CN): δ 1.00 (t, 36 H), 1.03 (s, 27 H), 1.41 (m, 24 H), 1.65 (m, 24 H), 3.15 (m, 24 H)

^{31}P NMR (CD_3CN): δ -16.95 (s, 1 P)

5.2.3 Synthesis of $[TBA]_3[PW_{10}O_{36}(^tBuSiO)_2VO(^iPrO)]$(PW10Si2VOPr)

0.402 g ($1.19x10^{-4}$ mol) of **PW10Si2** were placed in a Schlenk tube and heated at 215°C for 3 hours under vacuum. 4 mL of freshly distilled ACN and then 30 µL ($1.39x10^{-4}$ mol) of $VO(^iPrO)_3$ (the latter very slowly) were added, under argon atmosphere. The solution was stirred at room temperature overnight. The day after, 11 mL of fresh distilled and anhydrous diethyl ether were added extremely slowly, to allow the formation of two layers in the Schlenk tube and the crystallization of the product. After four days the formation of crystals was observed, and the solution was transferred in another Schlenk, under argon atmosphere. The crystals were collected under argon. Yield: 0.153 g, 37%

^1H NMR (CD_3CN): δ 1.00 (t, 36 H), 1.12 (s, 27 H), 1.41 (m, 24 H), 1.50 (d, 6 H), 1.65 (m, 24 H), 3.15 (m, 24 H), 5.65 (sept, 1 H)

^{31}P NMR (CD_3CN): δ -14.50 (s, 1 P)

^{51}V NMR (CD_3CN): δ -692 (s, 1 V)

5.2.4 Synthesis of $[TBA]_3[PW_9O_{34}(^tBuSiO)_3V]$ (PW9Si3V)

0.500 g ($1.53x10^{-4}$ mol) of **PW9Si3** were placed in a Schlenk tube, and heated at 215°C for 2 hours and 30 min under vacuum. 4 mL of freshly distilled ACN were added under argon atmosphere, and the resulting suspension was slowly heated to enhance solubility. Et_3N (0.074 mL, $5.36x10^{-4}$ mol) freshly distilled and then VCl_3*3THF (0.039 g, $1.68x10^{-4}$ mol) were added to the solution, ever under argon atmosphere. A dark blue solution was immediately obtained. The presence of some white solid on the bottom of Schlenk was eliminated by slowly heating at 60°C over night the reaction moisture. The day after, the product was precipitated with fresh distilled and anhydrous diethyl ether. The obtained solid was dried and then collected, under argon atmosphere.

^1H NMR (CD_3CN): δ 0.95 (s, 27 H), 1.00 (t, 36 H), 1.40 (m, 24 H), 1.65 (m, 24 H), 3.15 (m, 24 H)

5.2.5 Synthesis of $[TBA]_3[PW_9O_{34}(^tBuSiO)_3VO]$ (PW9Si3VO)

1 g ($3.06x10^{-4}$ mol) of **PW9Si3** was placed in a Schlenk tube, and heated at 215°C for 2 hours and 30 min under vacuum. 20 ml of freshly distilled ACN were added, and the Schlenk was placed at 0°C for 10 minutes. $VOCl_3$ (0.047 mL, $4.95x10^{-4}$ mol) was added, and the resulting limpid red/orange solution was stirred for 1 hour at 0°C under argon atmosphere. After that, the solution was left at room temperature over week-end. After

the week-end, the solution was concentrated up to few drops and crystallized with ether diffusion technique. The obtained crystals were grounded and dried at 40°C. Yield: 0.880 g, 86%

^{1}H NMR (CD_3CN): δ 1.00 (t, 36 H), 1.17 (s, 27 H), 1.40 (m, 24 H), 1.65 (m, 24 H), 3.15 (m, 24 H)

5.2.6 Synthesis of $[TBA]_3[PW_9O_{34}(^tBuSiO)_3ZrCl]$ (PW9Si3Zr)

1 g ($3.06x10^{-4}$ mol) of **PW9Si3** was placed in a Schlenk tube, and was heated at 215°C for 4 hours under vacuum. 5 mL of freshly distilled ACN were added under argon atmosphere, and the resulting suspension was slowly heated to enhance solubility. Freshly distilled Et_3N (0.140 ml, $1.01x10^{-3}$ mol) was added. $TiCl_4$ was dissolved in 3 mL of ACN under argon atmosphere in another Schlenk tube, and then the former solution was added drop-wise to the latter, ever under argon atmosphere. Formation of a heterogeneous white suspension was observed. The Schlenk was placed at 0°C for 15 minutes, and then stirred at room temperature over the week-end. The product was crystallized by means of acetone diffusion in ACN.

^{1}H NMR (CD_3CN): δ 1.00 (t, 36 H), 1.17 (s, 27 H), 1.40 (m, 24 H), 1.65 (m, 24 H), 3.15 (m, 24 H)

^{31}P NMR (CD_3CN): δ -15.60 (s, 1 P)

5.2.7 Reactivity of PW9Si3V with ethyl-2-diazoacetate

Ethyl-2-diazoacetate (diazo) (0.018 mL, $1.53x10^{-4}$ mol) was added to a solution of **PW9Si3V** (0.550 g, $1.53x10^{-4}$ mol) dissolved in 4 mL of freshly distilled ACN, under argon atmosphere. The solution colour changed from dark blue to brown. The solution was stirred at room temperature for one day. At the end, a dark brown solution was obtained. After NMR analysis, the product was dried and 10 mL of freshly distilled and anhydrous diethyl ether were added, to eliminate organic impurities.

^{1}H NMR (CD_3CN): δ 0.95 (s, 27 H), 1.00 (t, 36 H), 1.24 (t, 3 H), 1.40 (m, 24 H), 1.65 (m, 24 H), 3.15 (m, 24 H), 4.18 (q, 2 H), 4.98 (s, 1 H)

^{31}P NMR (CD_3CN): δ -14.78 (s, 1 P)

5.2.8 Reactivity of PW9Si3V with Styrene oxide

Styrene oxide (0.037 g, 3.06×10^{-4} mol) was added to a solution of **PW9Si3V** (1.10 g, 3.06×10^{-4} mol) dissolved in 4 mL of freshly distilled ACN, under argon atmosphere. No change of colour was observed. The solution was stirred at room temperature for one day, and after that it was heated at 60°C for three hours. The obtained solution was dark brown coloured.

The conversion of styrene oxide into styrene was determined by integration of the characteristic NMR resonances of the two products.

5.2.9 Catalytic oxidation tests

PW10Si2VOPr (0.016 g, 4.5×10^{-6} mol, 3% mol) was placed in an NMR tube under argon atmosphere, and dissolved with 0.5 mL of CD_3CN. After NMR analysis, 3-methylbut-2-en-1-ol (0.017 mL, 1.5×10^{-4} mol) was added. After NMR analysis, ^{t}BuOOH was added in the tube (0.027 mL, 1.5×10^{-4} mol, 5.5 M in decane) under argon atmosphere. The reaction evolution was monitored by ^{1}H, ^{31}P and ^{51}V NMR analyses.

Several other tests were carried out, varying the type of catalyst (**PW9Si3VO**, **PW9Si3, PW10Si2**, **VO(iPrO)$_3$**), its concentration (3% mol, 1% mol, 0.1% mol, 0.01% mol), the volume of ACN (0.5 mL or 3 mL) and the organic substrate (3-methylbut-2-en-1-ol or 1-hexene) (see below). All the tests were monitored by ^{1}H, ^{31}P and ^{51}V NMR analyses.

N. Test	*Catalyst*	*Catalyst Concentration (% mol)*	*ACN (mL)*	*Organic substrate*
1	**PW10Si2VOPr**	3%	0.5	3-methylbut-2-en-1-ol
2	**PW9Si3VO**	3%	0.5	3-methylbut-2-en-1-ol
3	**PW9Si3**	3%	3	3-methylbut-2-en-1-ol
4	**PW10Si2**	3%	3	3-methylbut-2-en-1-ol
5	**PW10Si2VOPr**	0.1%	3	3-methylbut-2-en-1-ol
6	**PW10Si2VOPr**	0.01%	3	3-methylbut-2-en-1-ol
7	**PW10Si2VOPr**	1%	3	1-hexene
8	**VO(iPrO)$_3$**	3%	0.5	3-methylbut-2-en-1-ol

5.2.10 Reactivity tests of POMs with hydroperoxyde

POM, 0.5 ml of CD_3CN and ^tBuOOH (0.027 ml, $1.5x10^{-4}$ mol, 5.5 M in decane) were added in the order in an NMR tube, under argon atmosphere.

Two different kinds of POM were utilized, **PW10Si2VOPr** (0.016 g, $4.6x10^{-6}$ mol, 3% mol), and **PW9Si3VO** (0.015 g, $4.6x10^{-6}$ mol, 3% mol). The evolution of the reaction was monitored by ^1H, ^{31}P and ^{51}V NMR analyses.

6. BIBLIOGRAPHY

[i] L. Mognon, Padova Universtiy, Master thesis (2011)

[ii] N.N. Greenwood, A. Earnshaw, “Chimica degli elementi”, **1992**, Piccin Nuova Libraria S.p:A., Padova

[iii]L. Mognon, Padova Universtiy, Master thesis (2011)

[iv] A. Proust et Al., *Chem. Soc. Rev.*, **2012**, *41*, pp. 7605-7622

[v] S. I. Allakhverdiev et Al., “Biomimetics, Learning from Nature”, Amitava Mukherjee (Ed.), **2010**

[vi] J. Clayden, N. Greeves, S. Warren, “Organic Chemistry”, Oxford University Press, Oxford, **2012**

[vii] G. Izzet et Al., *Inorg. Chem.*, **2011**, *50*, pp. 7761-7768

[viii] K.B. Sharpless, T.R. Verhoeven, *Aldrichchimica Acta*, **1979**, *12*, p. 63

1 M. T. Pope, A. Müller, “Polyoxometalates: from platonic solids to anti-retroviral activity”, Kluwer Academic Publisher, Dordrecht, **1993**

2 W. N. Lipscomb, *Inorg. Chem.*, **1965**, *4*, p. 132

3 M. T. Pope, “Polyoxometalates”, Georgetown University, Washington DC, USA

4 A. Hiskia et Al., *Chem. Soc. Rev*, **2001**, *30*, p. 62

5 N.N. Greenwood, A. Earnshaw, “Chimica degli elementi”, Piccin Nuova Libraria S.p.a., Padova, **1992**

6 J.J. Borras-Almenar et Al., *Polyoxometalates Molecular Science,* **2003**, *98*, pp. 33-54

7 J.J. Borras-Almenar et Al., *Polyoxometalates Molecular Science,* **2003**, *98*, pp. 3-31

8 A. Proust et Al., *Chem. Soc. Rev.*, **2012**, *41*, pp. 7605-7622

9 Jeffery D. Karcher, “Functionalized Polyoxometalates for Advanced Applications”, Phd Thesis, **2007**

10 J. E. Huheey, E. A. Keiter, R. L. Keiter, “Chimica Inorganica: Principi, Strutture, Reattività” Piccin Nuova Libraria S.p.a., Padova, **1999**

11 S. Stenbjörn, *Faraday Discuss*, **2012**, *155*, pp. 357-376

12 J. R. Bolton, “Solar Photoproduction of Hydrogen”, IEA Thecnical Report, **1996**

13 M. Carraro et Al., “Innovative Catalysis in Organic Synthesis: Oxidation, Hydrogenation and C-X Bond Forming Reactions”, Wiley-VCH Verlag GmbH & Co. KgaA., **2012**

14 C. Copéret et Al., *Angew. Chem., Int. Ed.*, **2003**, *42*, p. 156

15 A. Mazeaud et Al., *Inorg. Chem.*, **2000**, *39*, pp. 4735-4740

16 C. Copéret et Al., *Angew. Chem., Int. Ed.*, **2003**, *42*, pp. 173-175

17 G. Izzet et Al., *Chem. Sci.*, **2013**, *4*, p. 1737

18 G. Izzet et Al., *Energy Environ. Sci.*, **2013**, *6*, pp. 1504-1508

19 L. Ruhlmann et Al., *Dalton Trans.*, **2013**, *42*, p. 12688

20 G. Izzet, A. Proust et Al., *Chem. Commun.*, **2009**, pp 6062-6064

21 J. Clayden, N. Greeves, S. Warren, “Organic Chemistry”, Oxford University Press, Oxford, **2012**

22 K. Sonogashira et Al., *Tetrahedron Lett.*, **1975**, *16*, pp. 4467-4470

23 W. Zhang et Al., *Angew. Chem. Int. Ed.*, **2005**, *44*, pp. 4389-4391

24 F. Trifirò, F. Cavani, G. Centi, *Applied Catalysis*, **1984**, *9*, I*ssue 2*, pp. 191-202

25 G. Izzet et Al., *Inorg. Chem.*, **2011**, *50*, pp. 7761-7768

26 A. Mazeaud et Al., *Inorg. Chem.*, **2000**, *39*, pp. 4735-4740

27 A. Mazeaud, N. Ammari, F. Robert, R. Thouvenot, *Angew. Chem Int. Ed. Engl.*, **1996**, *35*, pp. 1961-1964

28 E. S. Gould et Al., *JACS*, **1968**, *90*, p. 4573

29 K. B. Sharpless et Al., *JACS*, **1973**, *95*, p. 6136